iScience

CellPress
OPEN ACCESS

Article

Single-cell fucosylation breakdown: Switching fucose to europium

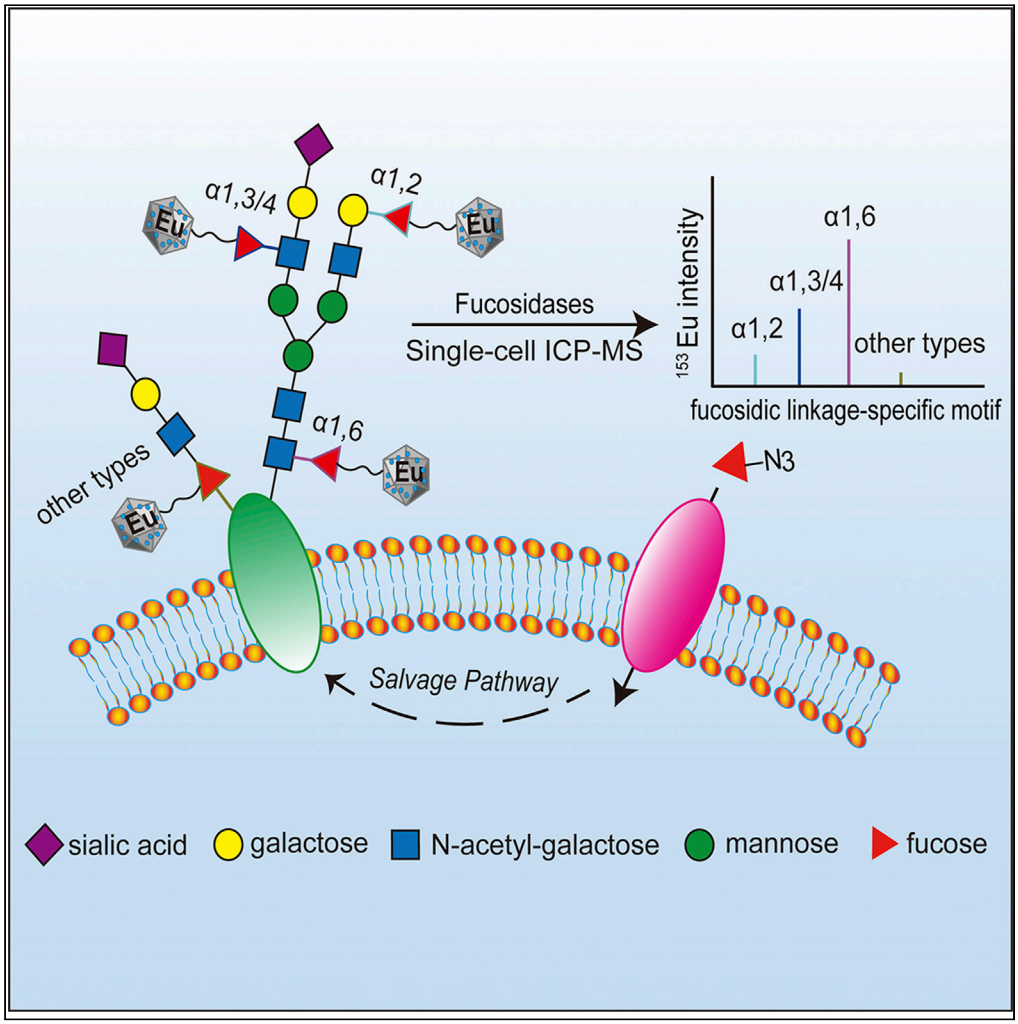

Zhen Liu, Yong Liang, Yang Zhou, Fuchun Ge, Xiaowen Yan, Limin Yang, Qiuquan Wang

qqwang@xmu.edu.cn

Highlights

Switching facile fucose to stable Eu mass signal on a single-cell ICP-MS platform

Ever lowest LOD of 4.2 zmol FucAz was achieved using a Eu-decorated MS2 nanoparticle

Single-cell breakdown of fucosidic linkage-specific motifs

Discrimination of highly, moderately, and poorly differentiated HCC from normal ones

Liu et al., iScience 24, 102397
May 21, 2021
https://doi.org/10.1016/j.isci.2021.102397

iScience

CellPress
OPEN ACCESS

Article

Single-cell fucosylation breakdown: Switching fucose to europium

Zhen Liu,[1] Yong Liang,[1] Yang Zhou,[1] Fuchun Ge,[1] Xiaowen Yan,[1] Limin Yang,[1] and Qiuquan Wang[1,2,*]

SUMMARY

Fucosylation and its fucosidic linkage-specific motifs are believed to be essential to understand their distinct roles in cellular behavior, but their quantitative information has not yet been fully disclosed due to the requirements of ultra-sensitivity and selectivity. Herein, we report an approach that converts fucose (Fuc) to stable europium (Eu) isotopic mass signal on hard ionization inductively coupled plasma mass spectrometry (ICP-MS). Metabolically assembled *azido*-fucose on the cell surface allows us to tag them with an *alkyne*-customized Eu-crafted bacteriophage MS2 capsid nanoparticle for Eu signal multiplication, resulting in an ever lowest detection limit of 4.2 zmol Fuc. Quantitative breakdown of the linkage-specific fucosylation motifs in situ preserved on single cancerous HepG2 and paracancerous HL7702 cells can thus be realized on a single-cell ICP-MS platform, specifying their roles during the cancering process. This approach was further applied to the discrimination of normal hepatocellular cells and highly, moderately, and poorly differentiated hepatoma cells collected from real hepatocellular carcinoma tissues.

INTRODUCTION

Cellular behavior is significantly governed by the biomacromolecules on the cell surface that carry meaningful information and serve biological functions, making the cells to be heterogeneous (Altschuler and Wu, 2010). During which, the linkage-specific multielement-composed motifs within the biomacromolecules direct their roles and eventually influence the cell behavior. Glycosylation is such a typical paradigm with diverse glycosidic linkages between monosaccharides attached covalently to their aglycone such as a protein and/or a lipid displaying various biological consequences (Ohtsubo and Marth, 2006; Pinho and Reis, 2015). For instance, fucosyltransferase (FUT)-mediated fucosylation on the cell surface has profound biological implications that depend heavily on its fucosidic linkages, such as α1,2-, α1,3/4-, and α1,6-linked fucosylation at the terminal, sub-terminal, and innermost core position of N-glycan chains, as well as the other types of fucosylation including O-fucosylation where fucose (Fuc) is added directly to Ser and Thr residue of, for example, epidermal growth factor-like repeats and thrombospondin type 1 repeats (Li et al., 2018; Ma et al., 2006; Schneider et al., 2017). These different fucosidic linkages donate diverse functions of fucosylation, saying that the α1,2-linkage Fuc is mainly responsible for A, B, and H Lewis blood antigens in blood type decision (Marionneau et al., 2001), while the α1,3/4 are believed to participate in the interactions between selectins and the α1,3/4-bearing sialyl-Lewis structures during many biological processes such as immune modulation and tumor metastasis (Barthel et al., 2009); as for the core α1,6, it has been deemed as a biomarker of cancer cells because its abnormal assembly always occurred during tumorigenesis (Aoyagi et al., 1991); as well as O-linked fucosylation promotes the metastasis of cancer by influencing protein folding, secretion, and in the regulation of Notch signaling (Taylor et al., 2014). Quantification of Fuc and more about its diversely fucosidic linkages have been placed at one of the central positions to unveil the causality between fucosylation and diseases (Li et al., 2018). Such diverse fucosidic linkage assemblies are catalyzed by their corresponding FUTs, therefore supposed in general from the perspective of biologists to be reflected by their corresponding FUTs' activity and abundance that could be detectably speculated by optical-based western blots electrophoretic methods and microarrays, but not the exact fucosidic linkage-specific motifs themselves (Chen et al., 2013; Mathieu et al., 2004; Yin et al., 2010). On the other hand, with the aid of the globally chemoselective and/or targeted biospecific enrichment procedures as well as related bioinformatics methods, information regarding monosaccharide composition and site- and glycan-specific glycosylation could be obtained using soft ionization tandem mass spectrometry (MS/MS), typically electrospray ionization Electrospray ionization-MS/MS and matrix-assisted laser

[1]Department of Chemistry & the MOE Key Lab of Spectrochemical Analysis and Instrumentation, College of Chemistry and Chemical Engineering, Xiamen University, Xiamen 361005, China

[2]Lead contact

*Correspondence: qqwang@xmu.edu.cn

https://doi.org/10.1016/j.isci.2021.102397

desorption/ionization matrix-assisted laser desorption/ionization-MS/MS, together with the sophisticated fragmentation strategies such as collision-induced dissociation (CID), electron capture dissociation, and electron transfer dissociation (Palaniappan and Bertozzi, 2016; Ruhaak et al., 2018). Definitely, collective knowledge contributed by the scientific forerunners built the contemporary comprehension about glycomics and glycoproteomics (Alley et al., 2013; Pinho and Reis, 2015). The state-of-the-art methodology developed, however, generally followed the apparently changeless steps toward the difficulties of (1) intrinsic poor and diverse ionization efficiency of the labile plus low abundance glycosylation and (2) awful heterogeneity raised from the branch-structured tree-shaped sugar chains with different glycosidic linkages of structural isomers. In-depth accurate information on the sequence and glycosidic linkages of a glycan is yet waiting to be fully disclosed, lying greatly on further improvements of MS tools and novel ion fragmentation strategies, in addition to the creation of richer structural library-based bioinformatics. Not just fucosylation exemplified here, it is a universally basic prerequisite to develop a methodology capable to distinguish and quantify not only total glycosylation but also the motifs assembled at different sites via different glycosidic linkages for exploring the structure-dependent roles of the glycosylated biomacromolecules on the cell surface. This still remains a challenge because an unfortunate problem is the unforeseeable cross-reactivity of the lectins used, besides the generally weak binding characteristics of the lectins toward specific glycosidic linkages for their recognition and enrichment (Cecioni et al., 2015; Ghazarian et al., 2011; Lis and Sharon, 1998). For example, the seemingly α1,6-selective *Aleuria aurantia lectin* displayed cross-reactivity toward multiple glycan epitopes including α1,2- and α1,3-linked Fuc (Noda et al., 2003). A more serious concern, on the other hand, is the facile Fuc ion migration and rearrangement behavior during the analysis of soft ionization MS/MS that unavoidably caused ambiguous even wrong results, despite chemical derivatization with easily ionized groups could overcome the issue of relative low ionization efficiency of Fuc (Harvey et al., 2002; Nwosu et al., 2015). Chemical modifications (Lattova et al., 2019) and fine controlling of the CID energy (Acs et al., 2018; Yuan et al., 2019b), for example, could minimize the consecutive processes of the facile Fuc ion migration and neutral Fuc residue loss during the soft ionization MS/MS enabling the discrimination of core and antenna fucosylation. But the sensitivity was reluctantly compromised, and still there were several (the core fucosylation) to a dozen (the antenna fucosylation) percentage of interferences, merely offering their relative abundance ratios if reference standard compounds were not available. Chemoenzymatic labeling strategies provided a selective approach but just limited to α1,2 Fuc linkage (Chaubard et al., 2012) being not able to provide a full spectrum of fucosylation on the cell surface.

Either in-source ionization and/or post-source fragmentation during the soft ionization MS/MS is a good manner that we initially expected making structure-dependent ionization and identification possible. However, in the same time, the soft ionization source is a gas-phase reactor that produces many unexpected fragment-ion rearrangement outcomes, causing a difficult situation that we do not want to see in the case of fucosylation analysis. Furthermore, the in situ scene of fucosylation and its linkage-specific motifs on the cell surface has been ever more desired to date, considering the fact that the glycosylated biomacromolecules integrated on a single cell is the most front line governing the heterogeneity of cellular behavior of cell-cell communication and immune modulation during normal and abnormal life processes, namely, the important cell profiling and cell-to-cell variability as we have already known (Pelkmans, 2012; Teichmann, 2019). Nonetheless, these not just qualitative but also quantitative information about the glycosidic linkage-specific motifs involved on a single cell are hard to be obtained not just because of the requirement of an unimaginable sensitivity but also because of the loss of the much desired in situ information on the cell surface when employing the current mainstream soft ionization MS/MS tools that generally analyze the cell lysates.

By contrast, Ar-based inductively coupled plasma (ICP) is a hard ionization source that converts most elements into their isotopic ions, especially the metallic elements that compose or are labeled to the biomacromolecules on an intact cell. When coupling to MS, inductively coupled plasma mass spectrometry (ICP-MS) is a universal tool not only for the quantification of the elements regardless of their chemical forms in which they exist (Montaser, 1998) but also for the biomacromolecules and cells via determination of the elements tagged (Bandura et al., 2009; Bendall et al., 2011; Li et al., 2005; Liang et al., 2015; Liu et al., 2016; Sanz-Medel et al., 2012; Virani and Tanner, 2015; Wei et al., 2020; Yan et al., 2013). If a monosaccharide, such as Fuc exemplified here, can be specifically tagged by a metallic element complex according to a certain stoichiometry, quantification of the Fuc would be switched to a genuine and credible isotopic mass signal of the element. The inevitable problem of the fragment ion rearrangements encountered during the soft ionization MS/MS would be fundamentally avoided. Moreover, ICP-MS is capable of directly analyzing intact cells and thus is able to directly readout the element-tagged Fuc

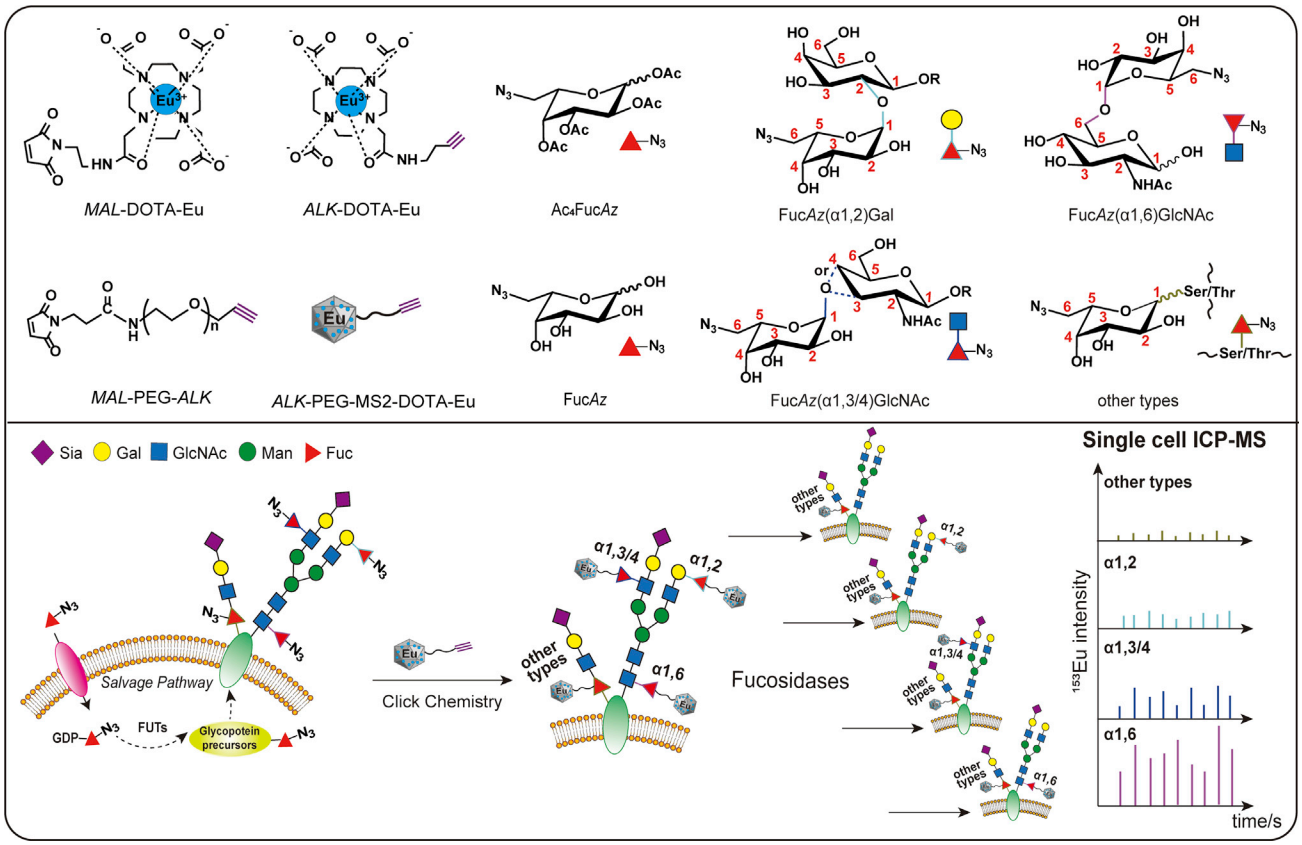

Scheme 1. Quantitative breakdown of single-cell fucosylation and its fucosidic linkage-specific motifs via a Eu-encoding single-cell ICP-MS approach mediated by globally metabolic assembly of FucAz via cell's essential salvage pathway and fucosidase-specific release strategy

Figure360▷ For a Figure360 author presentation of this figure, see https://doi.org/10.1016/j.isci.2021.102397.

The per-acetylated azide-fucose (Ac_4FucAz) was synthesized and used for incorporating FucAz into cell surface glycan chain via cell's essential fucose salvage pathway. Afterward, the globally incorporated FucAz on the single-cell surface can be recognized and conjugated bioorthogonally by an *ALK*-modified and Eu-decorated MS2 capsid nanoparticle element tag (*ALK*-PEG-MS2-DOTA-Eu) via click chemistry. In addition to the total fucosylation on a single cell, its linkage-specific motifs including terminal α1,2-, sub-terminal α1,3/4-, and innermost α1,6-linked fucosylation, as well as other types of fucosylation, can be accurately quantified via the determination of the tagged Eu using ^{153}Eu-species-unspecific isotope dilution ICP-MS on a single-cell ICP-MS platform with aid of the corresponding linkage-specific fucosidases.

in situ preserved on the cell surface upon a single-cell ICP-MS platform. In this study, we explored this capability for the quantitative breakdown of fucosylation and its linkage-specific motifs on a single cell (Scheme 1). Fortunately, post-modifiable Fuc analog such as per-acetylated azide-fucose (Ac_4FucAz) has been previously shown to be able to metabolically incorporate into the glycan chains and accumulate on the cell surface catalyzed by the cell's own *in vivo* FUTs via cell's essential salvage pathway (Rabuka et al., 2006; Sawa et al., 2006). This globally installed FucAz on the cell surface provides an opportunity to be bioorthogonally tagged by either an *alkyne* (*ALK*)-DOTA-europium (Eu) complex or *ALK*-modified and Eu-decorated bacteriophage MS2 capsid nanoparticle (*ALK*-PEG-MS2-DOTA-Eu) for Eu mass signal multiplication to meet the ultra-sensitivity requirement of a single-cell analysis. In addition to the total FucAz that enables better understanding of the difference between the different types of cells, selective quantification of trace amounts of the fucosidic linkage-specific motifs on a single cell can be achieved to elucidate heterogeneity among the same type of cells and thus the relationship between the linkage-specific motifs and their distinct biological functions, benefitted from linkage-specific fucosidase that can selectively detach its corresponding fucosidic linkage-specific motif from the cell surface glycan chain, while the wanted linkage-specific motif remains to be quantified. Human hepatocellular carcinoma HepG2 and paracancerous HL7702 cell lines were selected as the models of cancerous and normal cells to validate this proposed approach. Moreover, this approach was applied to the discrimination of highly, moderately, and poorly differentiated hepatoma cells from normal hepatocellular cells sampled from real hepatocellular carcinoma (HCC) and healthy liver tissues.

RESULTS AND DISCUSSION

Synthesis and characterization of Ac_4FucAz, *ALK*-DOTA-Eu, *MAL*-DOTA-Eu, and *ALK*-PEG-MS2-DOTA-Eu

We first synthesized the unnatural Ac_4Fuc*Az* according to the previous reports (Burkart et al., 2000; Laughlin and Bertozzi, 2007) with minor modifications (see transparent methods and Scheme S1). The intermediates and final product were characterized using ESI-qTOF-MS ($[M + Na]^+$ at m/z 396.0915, $[2M + Na]^+$ 769.1940) and ^{1}H-/^{13}C-NMR (Figures S1–S10), confirming the synthesis of Ac_4Fuc*Az* with a final yield of 47.5%. We next evaluated how the treatment with exogenous Ac4Fuc*Az* affects the cell growth status. As shown in Figure S11, the CCK-8 cytotoxicity assay indicated that the IC50 of Ac_4Fuc*Az* is 252.1 μM for HepG2 and 267.9 μM HL7702. Cell viability gradually decreases along with the increase in the concentration of Ac4Fuc*Az* in general with a plateau fluctuating around (79.3 ± 0.7) % of HL7702 and (82.6 ± 2.3) % HepG2 (n = 7) from 75 to 200 μM (Figure S11), which is in agreement with the phenomenon observed in other previous reports (Sawa et al., 2006; Hsu et al., 2007). In order to increase the cell uptake, thus for more efficacious incorporation of Fuc*Az* into the glycan chain on the cell surface, as well as to maintain stable cell growth status and obtain reproducible results, 200 μM Ac_4Fuc*Az* was used in the following cell culture experiments. Then, a Eu-loaded 1,4,7,10-tetraazacyclododecane-1,4,7-tris(acetic acid)-10-(3-butynylacetamide) (*ALK*-DOTA-Eu) complex (Figure S12, ESI-qTOF-MS $[M + H]^+$ at m/z 604.1601 and 606.1616) was synthesized and used to tag the Fuc*Az* metabolically incorporated on the cell surface for a bulk cell mode ICP-MS analysis. Meanwhile, a stoichiometrically Eu-decorated bacteriophage MS2 capsid nanoparticle was fabricated for Eu mass signal multiplication (Yuan et al., 2019a) to meet the ultra-sensitivity requirement for single-cell breakdown of fucosylation and its linkage-specific motifs on a direct infusion of lined up single-cell ICP-MS platform established in our lab (see Instrumentation of transparent methods) (Zhou et al., 2020). Different from our previous preparation route via the acylation between NHS-PEG_n-N_3 and the amino group (-NH_2) on the MS2 capsid nanoparticle and then clickable conjugation with a Eu-loaded 1,4,7,10-tetraazacyclododecane-1,4,7-tris(acetic acid)-10-dibenzocyclooctyne (*DBCO*-DOTA-Eu) (Yuan et al., 2019a), the active -NH_2 groups were firstly converted to sulfhydryl (-SH) groups using 2-iminothiolane hydrochloride (Traut's Reagent) for not only evading the possible hydrolysis of NHS under the experimental conditions but also adding an 8.1 Å spacer arm making -SH more flexible to be effortlessly modified (Figures 1A and 1B). The results obtained from ESI-qTOF-MS characterization before (MS2-NH_2 monomer with six modifiable -NH_2 groups at m/z 13,734.1438) and after modification (MS2-SH at m/z 14,339.9441) designated that the 1080 -NH_2 groups on the MS2 capsid nanoparticle were completely converted into 1080 -SH groups (Figure 1C). The observed transmission electron microscopy (TEM) size and morphology of the obtained MS2-SH did not noticeably change after the modification compared to those of MS2-NH_2 (27-nm spherical shell in diameter) (Figure 1D). Subsequently, the pre-synthetic Eu-loaded 1,4,7,10-tetraazacyclododecane-1,4,7-trisacetic acid-10-maleimidoethylacetamide (*MAL*-DOTA-Eu) (Luo et al., 2013; Yan et al., 2010, 2011) (Figure S13, ESI-qTOF-MS $[M + H]^+$ m/z 675.1367 and 677.1385) was employed to chemically craft MS2-SH via the Michael addition reaction between MAL and -SH. The obtained results using ^{153}Eu-species-unspecific isotope dilution ICP-MS (^{153}Eu-SUID-ICP-MS) coupled with size-exclusion chromatography (SEC) (Figure S14A) indicated that all the -SHs can be quantitatively modified, suggesting that 1080 Eu atoms were chemically decorated on one MS2 capsid nanoparticle (MS2-DOTA-Eu). Moreover, in order to impart the tagging ability of MS2-DOTA-Eu toward the Fuc*Az* on the cell surface, a 45-ethylene glycol unit containing PEG-linked (PEG2000, 157.5 Å in length) *MAL*-PEG2000-*ALK* (171.6 Å) was used to chemically modify MS2-SH for (1) merely reacting with the outer surface of -SHs because the capsid pores of 18 Å prevent the *MAL*-PEG2000-*ALK* from entering into the interior of MS2 capsid and (2) protruding *MAL*-PEG2000-*ALK* outside the surface of the MS2-DOTA-Eu far beyond *MAL*-DOTA-Eu (13.5 Å). Such a design could avoid the electrostatic repulsion and steric hindrance effects, thus benefiting the bioorthogonally clickable tagging of the Fuc*Az* on the cell surface. The number of *MAL*-DOTA-Eu and *MAL*-PEG2000-*ALK* that have the same reactive group *MAL* toward -SH could be tuned via changing their molar ratio from 1/2 to 0/1, resulting in (471 ± 16) to (1080 ± 27) of *MAL*-DOTA-Eu and (609 ± 16) to (0 ± 27) of *MAL*-PEG2000-*ALK* (n = 7) on one MS2 determined using SEC-^{153}Eu-SUID-ICP-MS (Figures S14B–S14H). Compared with PEG600 (14 ethylene glycol units, 49.0 Å), PEG1000 (23, 80.5 Å), PEG3400 (77, 269.5 Å), and PEG5000 (114, 399 Å) tested, ALK_{101}-PEG2000-MS2-DOTA-Eu_{979}, which was obtained at the molar ratio of 1/50 of *ALK*-PEG2000-*MAL* to *MAL*-DOTA-Eu, not only guaranteed the tagging ability toward the Fuc*Az* but also demonstrated the highest signal multiplication up to (979 ± 15) times (n = 7). In this way, nearly three orders of magnitude higher ^{153}Eu isotopic mass signal intensity was improved than merely using *ALK*-DOTA-Eu (Figures S15 and S16). The limit of detection (LOD) of Fuc*Az* is down to 16.1 amol (corresponding to 9.7×10^6 Fuc*Az*) compared with 15.6 fmol (9.4×10^9 Fuc*Az*) using

ALK-DOTA-Eu alone (Figure 1E), which was calculated by 3 × SD dividing the slope of the corresponding calibration curves, given the fact that the clickable 1:1 conjugation between -ALK and -N_3 (Figure S17) via the bis[(tertbutyltriazoyl)methyl]-[(2-carboxymethyltriazoyl)methyl]-amine (BTTAA) mediated Cu(I)-catalyzed azide-alkyne cycloaddition during which BTTAA and aminoguanidine were used for stabilizing and detoxicating the cytotoxicity of Cu(I) (Besanceney-Webler et al., 2011; Uttamapinant et al., 2012).

Metabolic incorporation and quantification of the total Fuc*Az* on single cell surface

Human HCC and paracancerous cell lines HepG2 and HL7702 were selected as the models of cells. They were cultivated in the presence of 200 μM Ac_4Fuc*Az*. Afterward, the cells were tagged using *ALK*-DOTA-Eu. We found that only the cells cultured with Ac_4Fuc*Az* were determined by ICP-MS when monitoring $^{151/153}$Eu, while those without Ac_4Fuc*Az* cultivation and/or *ALK*-DOTA-Eu tagging detected with almost negligible background signal (Figure S18). These results suggested the success of the metabolic incorporation of Fuc*Az* on the cell surface and the specificity of the clickable *ALK*-DOTA-Eu tagging. In parallel, *ALK*-Cy5 with the same reactive *ALK* group as *ALK*-DOTA-Eu was used to label the cells. The confocal laser scanning microscope observation confirmed the same results (Figure S19) but could hardly offer the quantitative content of Fuc*Az* on the cell surface. The total Fuc*Az* can be quantified using ^{153}Eu-SUID-ICP-MS under a bulk cell mode using a dwell time of 100 ms with a cell population of 1.0 × 10^6 HepG2 and/or HL7702. The average contents of the Fuc*Az* per HepG2 and HL7702 that were calculated by the total FucAz determined dividing the cell number used are (8.3 ± 0.3) × 10^{-17} mol (corresponding to 5.0 × 10^7 Fuc*Az*) and (8.4 ± 0.4) × 10^{-18} mol (5.1 × 10^6 Fuc*Az*) (n = 7) according to the calibration curves (Figure 1E), indicating that more than one order of magnitude higher Fuc*Az* incorporated on HepG2 than HL7702. These results also implied that at least 187 HepG2 and 1848 HL7702 cells are needed under the bulk cell mode ICP-MS analysis using *ALK*-DOTA-Eu tag for direct readout of the Fuc*Az* considering the LOD of 15.6 fmol Fuc*Az* and the average Fuc*Az* contents on the cells, being far away from the ultra-sensitivity requirement for an exact single-cell analysis. When ALK_{101}-PEG2000-MS2-DOTA-Eu_{979} was used to tag the cells, by contrast, one HepG2 and two HL7702 cells could be determined owing to the signal-multiplicated LOD of 16.1 amol. It should be noted that when the cells were analyzed on the single-cell ICP-MS platform with the 10-fold shorter dwell time of 10 ms than that used in the bulk cell mode, the signal to noise ratio could be further improved, resulting in the LOD down to 4.1 amol Eu (Figure S20). Taking the advantage of signal multiplication effect of ALK_{101}-PEG2000-MS2-DOTA-Eu_{979}, 4.2 × 10^{-21} mol (zmol) Fuc*Az* (corresponding to 2.5 × 10^3 Fuc*Az*) can be detected, guaranteeing the direct readout of a real single-cell event regarding not only the total Fuc*Az* but also its linkage-specific motifs on the single-cell ICP-MS platform (Figures 2A, S21, and S22), which could line up single cells with a controllable adjacent interval time and directly infuse them one by one into ICP-MS with the almost quantitative transport efficiency and detection efficiency of 86%. The average Fuc*Az* of (8.3 ± 0.6) × 10^{-18} mol (corresponding to 5.0 × 10^6 Fuc*Az*) per HL7702 cell and (8.4 ± 0.5) × 10^{-17} mol (5.1 × 10^7 Fuc*Az*) HepG2 determined from the 3000 independent single-cell events of each run (n = 21) are comparable to those obtained under the bulk cell mode analysis (Figure 2B). The signal multiplication ALK_{101}-PEG2000-MS2-DOTA-Eu_{979} nanoparticle tag allowed us to determine the single-cell events and distinguish either HepG2 from HL7702 cells or cell-to-cell heterogeneity among the same HepG2 and/or HL7702 cells regarding fucosylation (Figures 2B and 2C). The statistical results obtained (Figure 2C) indicated that the Fuc*Az* content per HL7702 cell ranges from (4.8 ± 0.7) × 10^{-18} (10% limit) to (1.3 ± 0.4) × 10^{-17} mol/cell (90% limit), being difference of 2.7 times with the average and median values of (8.3 ± 0.6) × 10^{-18} mol/cell and (7.8 ± 0.7) × 10^{-18} mol/cell; while on HepG2, the Fuc*Az* content ranges from (2.8 ± 0.6) × 10^{-17} (10%) to (1.5 ± 0.3) × 10^{-16} mol/cell (90%) of 5.4 times difference with the average and median values of (8.4 ± 0.5) × 10^{-17} mol/cell and (6.6 ± 0.4) × 10^{-17} mol/cell. Not only more than 10-fold higher Fuc*Az* content on HepG2 than HL7702 according to the average value of the total Fuc*Az* ($p < 0.001$, n = 21) (Figure 2B), but also 2-fold larger heterogeneity of HepG2 than HL7702 in general (Figure 2C). These results also revealed that not all HL7702 cells incorporated lower levels of Fuc. Around 2% of the paracancerous HL7702 cells did express abnormally high levels of Fuc*Az* (>1.8 × 10^{-17} mol/cell) that overlapped with some of HepG2, implying that these paracancerous cells might have the tendency to be tumorigenesis. Among the more heterogeneous HepG2 cells, there are merely 1% hepatoma carcinoma cells which incorporated extremely higher amount of Fuc*Az*, 1.9-fold higher than the average amount of Fuc*Az* on the cell colony based on the 99% confidence, providing experimental evidence for the speculation that only a few cancerous cells play more invasive notorious roles during cancer metastasis even though they are all belonging to the same HepG2 cell line. Clearly, such information uncovered by ALK_{101}-PEG2000-MS2-DOTA-Eu_{979} signal multiplication single-cell ICP-MS analysis would be hidden in the bulk cell ensemble analysis.

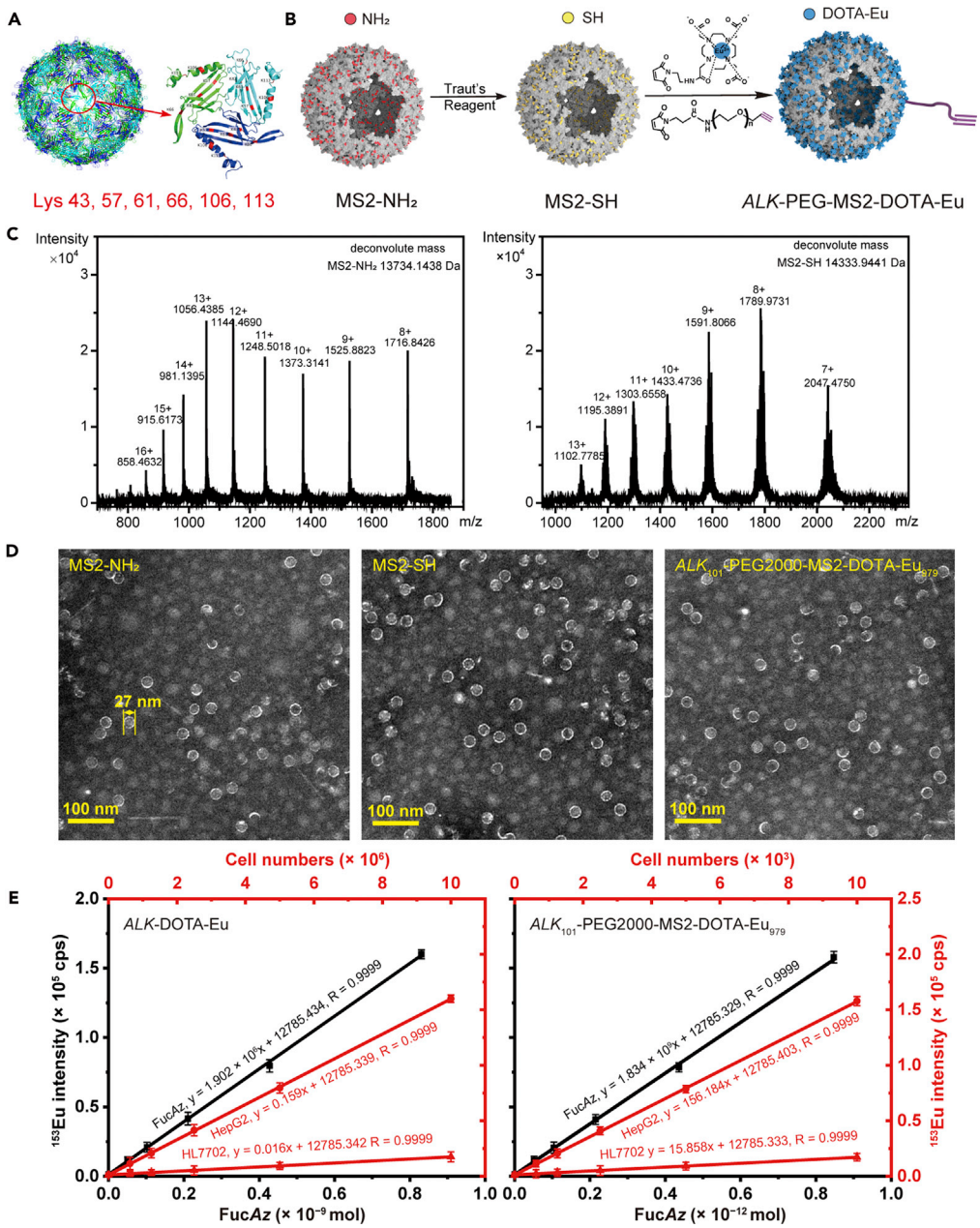

Figure 1. Preparation, characterization, and application of Eu-decorated bacteriophage MS2 capsid signal multiplication nanoparticle tag

(A) Bacteriophage MS2 is composed of 180 identical protein monomers, and each monomer has six modifiable amino sites, thus totally 180 × 6 = 1080 amino sites can be chemically modified;

(B) The preparation routes of *ALK*-PEG-MS2-DOTA-Eu via two key steps including the conversion of -NH_2 to -SH using Traut's Reagent and -SH conjugation with *MAL*-DOTA-Eu and *MAL*-PEG-*ALK* for Eu mass signal amplification and targeting the Fuc*Az* metabolically assembled in the glycan chains on the cell surface;

(C) ESI-qTOF-MS of MS2-NH_2 capsid monomer at m/z 13,734.1438 and MS2-SH 14339.9441;

(D) TEM images of MS2-NH_2, MS2-SH, and ALK_{101}-PEG2000-MS2-DOTA-Eu_{979} nanoparticles, scale bar, 100 nm;

(E) Calibration curves of ^{153}Eu-ICP-MS intensity ($^{153}Eu_{spike}$ × 99.8% + $^{153}Eu_{Sample}$ × 52.19%) against the Fuc*Az* amount (left y and bottom x) and cell number of HL7702 and HepG2 (right y and top x) tagged with *ALK*-DOTA-Eu and ALK_{101}-PEG2000-MS2-DOTA-Eu_{979} (n = 7, data are represented as mean ± SD).

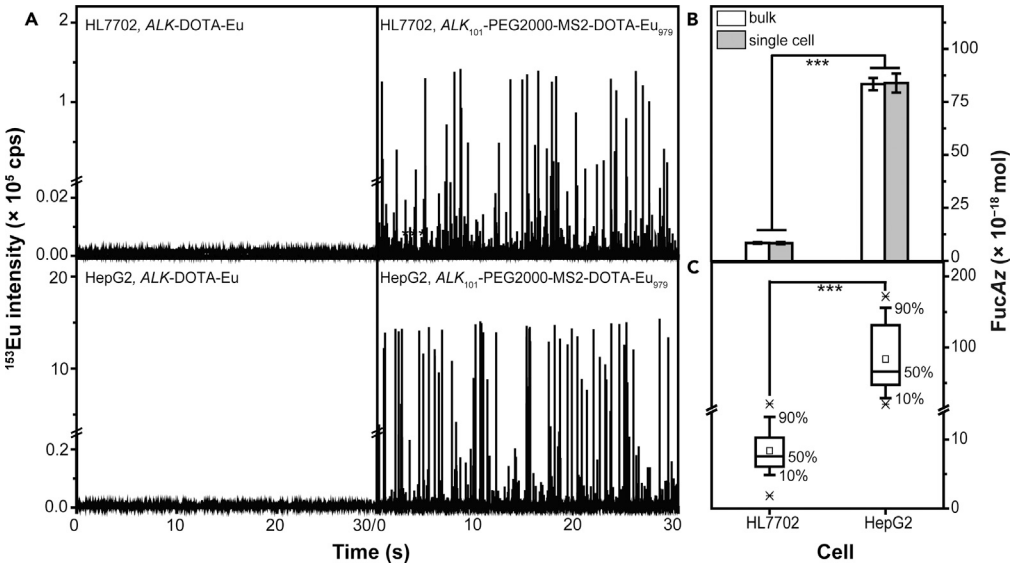

Figure 2. Quantification of the total FucAz on the single-cell surface via single-cell ICP-MS

(A) Single-cell analysis of HL7702 and HepG2 tagged with *ALK*-DOTA-Eu and ALK_{101}-PEG2000-MS2-DOTA-Eu_{979} from 3000 independent single-cell events on the single-cell ICP-MS platform;

(B) Statistical significance of FucAz between HL7702 and HepG2 evaluated from 3000 independent single-cell events of each run (n = 21) under the bulk cell analysis and single-cell ICP-MS based on the average FucAz values with *t* test, $p < 0.001$ (n = 21, data are represented as mean ± SD).

(C) Box chart for illustrating heterogeneity regarding the total FucAz on single HL7702 and HepG2 cells derived from 3000 single-cell events, in which the percentile line of the box chart was set at the segments of 10%, 25%, 50%, 75%, and 90%; the square inside denotes the average value and the line, the medium value; statistical significance of the FucAz between HL7702 and HepG2 with *t* test, $p < 0.001$ (n = 21).

Quantitative breakdown of the fucosidic linkage-specific motifs on a single cell and their bioclinical implications

In addition to the total FucAz, quantitative information on its fucosidic linkage-specific motifs might provide in-depth insights for the evaluations of the different biological behavior between HepG2 and HL7702. Employing the linkage-specific fucosidases (Gotz et al., 2014; Yan et al., 2018), the fucosylation linkage-specific motifs on a single cell can be uncovered on the single-cell ICP-MS platform via ALK_{101}-PEG2000-MS2-DOTA-Eu_{979} tagging (Figure S22). Firstly, the other types of fucosylation including O-fucosylation on HL7702 and HepG2 were quantified after removing the α1,2, α1,3/4 and α1,6 linkage motifs using their corresponding fucosidases together. The absolute content on HL7702 ranging from $(1.0 \pm 0.3) \times 10^{-19}$ (10%) to $(3.4 \pm 0.4) \times 10^{-19}$ mol/cell (90%) was determined from the 3000 valid cell events of each run (n = 21) with the average and medium values of $(1.9 \pm 0.5) \times 10^{-19}$ mol/cell and $(1.7 \pm 0.4) \times 10^{-19}$ mol/cell, while those on HepG2 from $(8.9 \pm 1.5) \times 10^{-19}$ (10%) to $(2.7 \pm 0.3) \times 10^{-18}$ mol/cell (90%) with average and medium of $(1.3 \pm 0.4) \times 10^{-18}$ mol/cell and $(1.1 \pm 0.3) \times 10^{-18}$ mol/cell. Average amounts of the other types account for (2.3 ± 0.6)% on HL7702 and (1.6 ± 0.5)% on HepG2 of the total FucAz (Figures 3A and 3B). Although the relative proportion on HepG2 is 0.7% lower than that on HL7702, the absolute content on HepG2 is 6.8-fold higher. This result implies the other types of fucosylation, including the O-linked fucosylation that is in charge of Notch signaling, might play certain roles during carcinogenesis processes (Taylor et al., 2014). Next, we used α1,3/4- and α1,6-specific fucosidases together to cleave α1,3/4- and α1,6-linked Fuc out of the cell-surface, the remained α1,2-linked FucAz was quantified ranging from $(4.5 \pm 1.1) \times 10^{-19}$ mol (10%) to $(1.5 \pm 0.4) \times 10^{-18}$ mol (90%) per HL7702 cell with the average and medium values of $(8.8 \pm 1.6) \times 10^{-19}$ mol/cell and $(8.5 \pm 1.3) \times 10^{-19}$ mol/cell by subtracting that of the other types of FucAz linkage-specific motifs, while $(1.4 \pm 0.3) \times 10^{-18}$ (10%) to $(5.7 \pm 0.4) \times 10^{-18}$ mol (90%) per HepG2 cell with average and medium values of $(2.5 \pm 0.2) \times 10^{-18}$ mol/cell and $(2.1 \pm 0.3) \times 10^{-18}$ mol/cell were determined, indicating that 1.2 times more heterogeneous and 2.8-fold higher α1,2-linkage FucAz metabolically incorporated on HepG2 than HL7702 (Figure 3A). It was also interesting to find that the relative percentage of (10.6 ± 1.9)% of α1,2-linkage FucAz on HL7702 is inversely 3.5-fold higher than (3.0 ± 0.3)% on HepG2 (Figure 3B). These high absolute contents but low relative percentages of α1,2-linkage FucAz on HepG2 compared with HL7702 might be one of the possible reasons for the contradictory results reported so far about

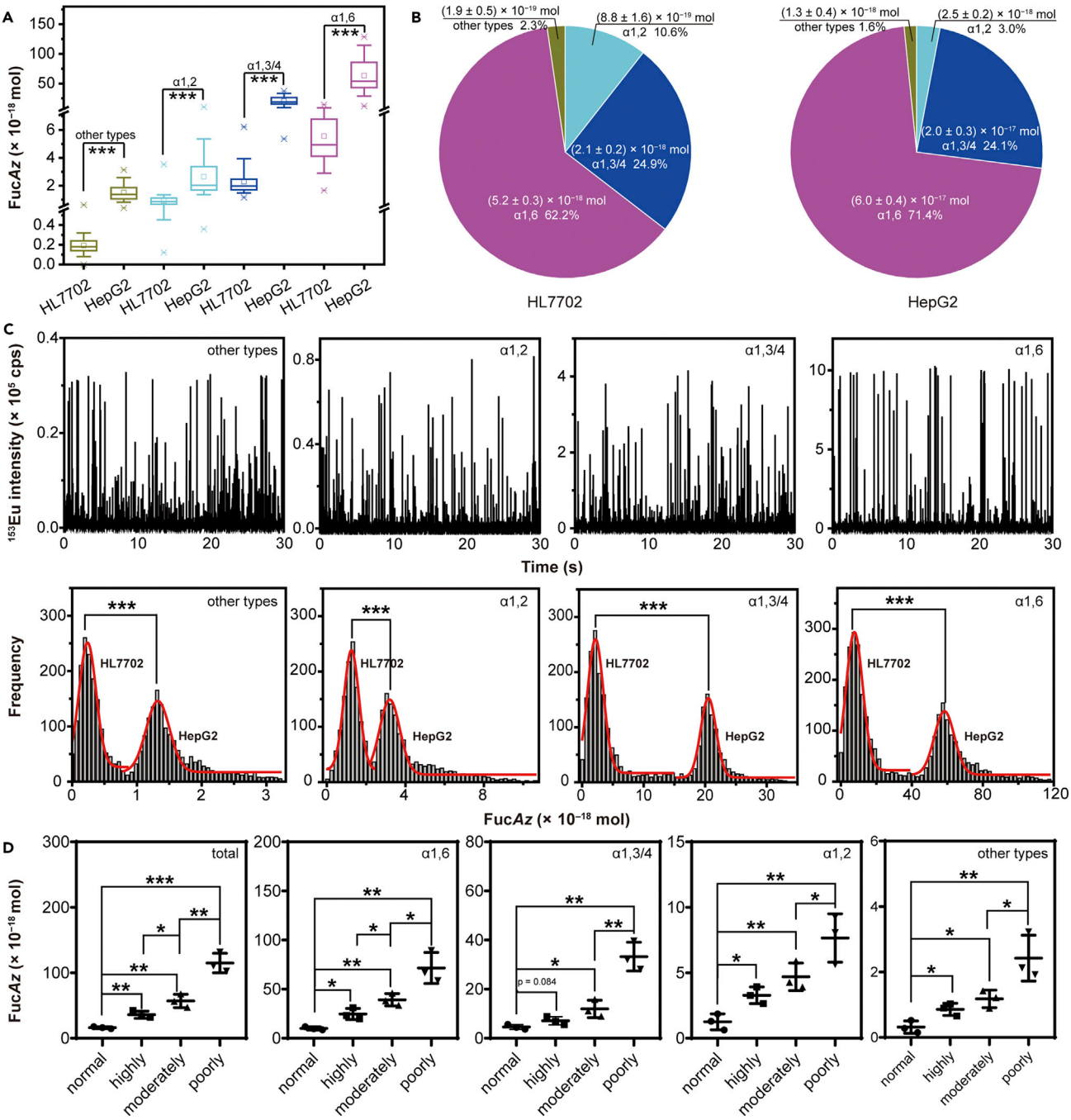

Figure 3. Quantification and breakdown of the fucosidic linkage-specific motifs on a single cell

(A) Box chart of the α1,2, α1,3/4, α1,6 and other linkage-specific fucosylation illustrates the difference between HL7702 and HepG2 and the cell-to-cell heterogeneity among the same type of HL7702 and/or HepG2, in which the percentile line was set in the segments of 10%, 25%, 50%, 75%, and 90%, and the inside square denotes the average value and the line, the medium. Statistical significance of the different FucAz linkage-specific motifs between HL7702 and HepG2 with *t* test from the 3000 valid single-cell events of each run, $p < 0.001$ (n = 21);

(B) Breakdown of the α1,2, α1,3/4, α1,6 and other linkage-specific FucAz on the single cell of HL7702 and HepG2;

(C) Screening of cancerous HepG2 from paracancerous HL7702 in the mixture of HepG2 and HL7702 cells based on the α1,2; α1,3,4; α1,6 and other linkage-specific fucosylation motifs on the single-cell ICP-MS platform from 3000 valid single-cell events, $p < 0.001$, (n = 21).

(D) Average FucAz contents of the total and linkage-specific motifs on the single-cell surface of clinically resected liver tissues of 12 patients including 3 normal liver and 3 highly, 3 moderately, and 3 poorly differentiated HCC cells determined on the single-cell ICP-MS platform from 3000 valid single-cell events of five replicated runs (n = 5).

its speculated functions on different kinds of cells that need to be further investigated (Belo et al., 2015). Anyway, unlike the previously reported relative quantification either by using lectin-immobilized columns and then with enzyme-linked immunosorbent assay or via the detection of fucosyltransferase activity to indirectly reflect α1,2-linkage Fuc from the cell lysates (Mathieu et al., 2004), the absolute quantity of α1,2-linkage Fuc*Az* was exactly determined on the intact single HepG2 and HL7702 cells, providing a much more solid evidence of α1,2-linked fucosylation playing important roles during tumorigenesis, besides its well-known role in the decision of A, B, and H blood type (Fukushima et al., 2009; Marionneau et al., 2001). Similarly, the absolute contents of α1,3/4-linked Fuc*Az* on HL7702 and HepG2 were quantified being from $(1.6 \pm 0.3) \times 10^{-18}$ (10%) to $(4.0 \pm 0.5) \times 10^{-18}$ mol per HL7702 cell (90%) and $(1.0 \pm 0.3) \times 10^{-17}$ to $(3.2 \pm 0.4) \times 10^{-17}$ per HepG2 cell with the average and medium values of $(2.1 \pm 0.2) \times 10^{-18}$ mol and $(2.0 \pm 0.4) \times 10^{-18}$ mol for HL7702 and $(2.0 \pm 0.3) \times 10^{-17}$ mol HepG2 and $(1.9 \pm 0.3) \times 10^{-17}$ mol for HepG2, respectively. Although 10-fold lower α1,3/4-linked Fuc*Az* content on HL7702 than HepG2 with 3.2 times heterogeneity of HepG2 cells and 2.5 HL7702 (Figure 3A) was found, the relative proportion of the average contents of (24.9 ± 2.5)% on HL7702 and (24.1 ± 3.4)% HepG2 was almost the same (Figure 3B). These results suggested again that the absolute content of α1,3/4-linked Fu*cAz* on the cell surface dominates more significant roles as thinking about the fact that some sialyl Lewis antigens, especially the overexpressed α1,3/4-linkage fucosylation-bearing sialyl Lewis^{x} and sialyl Lewis^{a}, interact more tightly with the selectin molecules, one possible reason leading to the slower rolling speed of cancer cells along the vascular endothelium, thus enhancing the ability of the so-called circulating tumor cells to extravasate from the vasculature into surrounding tissues (Barthel et al., 2009; Yin et al., 2010). About 2% of HL7702 cells overlapped with HepG2 ($> 5.4 \times 10^{-18}$ mol/cell) and, 1% HepG2 was 1.7-fold higher than the average Fuc*Az* of the HepG2 cell colony. Such a small portion with ultrahigh α1,3/4 Fuc*Az* on HL7702 and HepG2 might be an implication of either a few of the paracancerous HL7702 cells being prone to tumorigenesis or only a few of the cancerous HepG2 playing notorious roles during cancer metastasis like cancer stem cells (Barkeer et al., 2018). As for the innermost α1,6-linked Fuc*Az*, its absolute content was quantified being $(2.9 \pm 0.3) \times 10^{-18}$ (10%) to $(9.1 \pm 0.6) \times 10^{-18}$ (90%) with the average and medium values of $(5.2 \pm 0.3) \times 10^{-18}$ mol and $(5.1 \pm 0.3) \times 10^{-18}$ mol per HL7702, accounting for (62.2 ± 3.3)% of the total Fuc*Az*; while $(2.5 \pm 0.4) \times 10^{-17}$ to $(1.1 \pm 0.3) \times 10^{-16}$ with the average and medium values $(6.0 \pm 0.4) \times 10^{-17}$ mol/cell and $(5.8 \pm 0.5) \times 10^{-17}$ mol/cell accounting for (71.4 ± 5.0)% on HepG2. The absolute value on HepG2 is nearly 12-fold higher than that on HL7702 and the relative proportion is 9.2% higher than that of HL7702 ($p < 0.001$, $n = 21$) (Figures 3A and 3B). These straightforward results showed that not only the absolute amount but also relative proportion of α1,6-linked Fuc*Az* is higher on HepG2, convincingly indicating that α1,6-linked Fuc plays a critical role in cancer tumorigenesis, invasion, and cancer metastasis processes. The quantitative outcomes are well in accordance with the consensus that extremely high incorporation of the α1,6-linked fucosylation always occurred during tumorigenesis, recognizing as a biomarker of cancer (Taylor et al., 2014; Wang et al., 2015). Furthermore, 1% of the cancerous HepG2 displayed 1.9-fold higher Fuc*Az* than the average Fuc*Az* content of the cell colony, suggesting again that just a small portion of the cancerous cells playing efficacious roles in the process of invasion and metastasis. Taken together, the relative proportions and especially the absolute contents of the different linkage-specific Fuc*Az* motifs discovered on the intact single cell of HepG2 and HL7702 dig up more concealed fucosylation linkage-specific motifs information compared to the previously employed techniques (such as ESI-MS/MS and MALDI-MS/MS and lectin-based glycan array) that analyze the cell lysates of an ensemble population of cells (Acs et al., 2018; Moriwaki and Miyoshi, 2010). However, it is worthy of pointing out that the different fucosidic linkage-specific motifs must not execute independently but synergistically carry out a cellular action. More detailed investigation by professional biologists will be absolutely needed using the single-cell fucosylation breakdown methodology we developed as well as the single-cell fucosylation and its fucosidic linkage-specific motifs information we provided here.

The discrepancy in the absolute contents of not only the total fucosylation but also different fucosylation linkage-specific motifs on the single cell can be further utilized to distinguish the cancerous HepG2 from the cell mixture of HepG2 and the paracancerous HL7702 cells ($p < 0.001$, $n = 21$) on the single-cell ICP-MS platform (Figure 3C), which would be advancing for the early targeted screening of cancer. Furthermore, we applied this developed approach to the real samples of the normal liver and variously differentiated HCC tissues including highly, moderately, and poorly differentiation HCC collected from Xiamen University Affiliated Zhong Shan Hospital. In addition to the clear discrimination between normal [$(1.6 \pm 0.1) \times 10^{-17}$ mol/cell] and highly [$(3.6 \pm 0.5) \times 10^{-17}$ mol/cell] ($p < 0.01$), moderately [$(5.7 \pm 1.0) \times 10^{-17}$ mol/cell] ($p < 0.01$), and poorly [$(1.1 \pm 0.1) \times 10^{-16}$ mol/cell] ($p < 0.001$) differentiated HCC cells, using the average total FucAz contents determined on the single cells with $p < 0.05$ for highly and moderately and $p < 0.01$ for moderately and poorly ($n = 5$) differentiated HCC cells (Figure 3D), the linkage-specific motifs as well can distinguish not only the poorly and moderately but also

highly differentiated HCC cells from the normal ones. Among them, the average Fuc*Az* content of α1,6 linkage-specific motif could discriminate the normal liver cells from the highly differentiated HCC cells with $p < 0.05$, the moderately ($p < 0.01$) and the poorly ($p < 0.01$) as determined being $(1.0 \pm 0.2) \times 10^{-17}$ mol per normal liver cell, $(2.5 \pm 0.6) \times 10^{-17}$ mol highly, $(3.9 \pm 0.6) \times 10^{-17}$ mol moderately, and $(7.2 \pm 1.6) \times 10^{-17}$ mol poorly differentiated HCC; and the highly and moderately were distinguished with $p < 0.05$ and, the moderately and poorly $p < 0.05$. Based on the average α1,2 Fuc*Az* of $(1.3 \pm 0.6) \times 10^{-18}$ mol/cell on the normal cell and $(3.3 \pm 0.6) \times 10^{-18}$ mol/cell the highly, they could be distinguished with $p < 0.05$; the 3.6- and 5.9-fold up-regulated α1,2 Fuc*Az* on the moderately and poorly differentiated HCC cells compared with the normal tissue, resulting in a statistically significant difference of $p < 0.01$ between the normal and the moderately and/or the poorly. It is worth noting that the average α1,3/4 Fuc*Az* content could discriminate the normal $(4.6 \pm 1.0) \times 10^{-18}$ mol/cell from the poorly ($(3.3 \pm 0.6) \times 10^{-17}$ mol/cell) with $p < 0.01$ and the moderately ($(1.2 \pm 0.4) \times 10^{-17}$ mol/cell, $p < 0.05$), but less significant difference of $p = 0.084$ for classifying the normal from the highly differentiated HCC cells ($(7.1 \pm 1.7) \times 10^{-18}$ mol/cell). Such results might be ascribed to that the function of α1,3/4Fuc*Az* was supposed to be in charge of the interactions between the α1,3/4-bearing sialyl-Lewis structures and selectins during tumor metastasis, which overexpressed at the poorly differentiated stage of HCC (Barthel et al., 2009). Anyway, compared with biopsies and tissue imaging that examine advanced cancer (Wald et al., 2013) and sera biomarkers (Adamczyk et al., 2012) such as AFP, CEA, CA125, and CA199 which frequently encounter the false-positive or false-negative outcomes (Table S1), the total Fuc*Az*, α1,6 and α1,2 fucosydic linkage-specific motifs contents can unambiguously discriminate highly differentiated HCC cells from the normal liver cells, in addition to the discrimination between the normal and the moderately or the poorly differentiated HCC cells. This is very significant supporting the early diagnosis and surveillance of HCC.

Conclusion

Thanks to the cell's essential salvage pathway that mediates Fuc*Az* incorporation into the cell surface glycan chain, we are able to use an ALK_{101}-PEG2000-MS2-DOTA-Eu_{979} signal multiplication nanoparticle for tagging and reporting the Fuc*Az* on a single cell. The conversion of Fuc*Az* to $^{153}Eu^{+}$ mass signal determined using ICP-MS not only avoided the inevitable Fuc ion rearrangements encountered during the soft ionization MS/MS but also provided in situ fucosylation information on an intact cell. Almost 1000 Eu atoms decorated on the ALK_{101}-PEG2000-MS2-DOTA-Eu_{979} deliver an ever lowest detection limit of 4.2 zmol Fuc*Az*, allowing the quantification of the total Fuc*Az* and the quantitative breakdown of the linkage-specific fucosylation in situ on a single cell on the single-cell ICP-MS platform, uncovering the cell-to-cell heterogeneity. Even though the total Fuc*Az* revealed by the approach developed here just accounts for (11.8 ± 0.3) % on HepG2 and (8.4 ± 0.4) % HL7702 ($n = 3$) of the "whole fucosylation" that metabolically incorporated via both of the cell's own salvage and de novo pathways, which could be determined using the cell-lysed standard monosaccharide 1-Phenyl-3-methyl-5-pyrazolone (PMP)-derivatization and HPLC method (Figure S23), the new findings discovered on the fucosidic linkage-specific motifs on cancerous HepG2 and paracancerous HL7702 cells do provide more insights that specify their distinct roles on the cellular behavior regarding a cancering process.The capability demonstrated to distinguish the cancerous cells from the normal ones supports the surveillance and diagnosis of cancer. Distinct functions of the biomacromolecules with isomerically linkage-specific glycosylation motifs governing the marked behavior of biomacromolecule-integrated cells are universal phenomena, not limited to the cell's fucosylation demonstrated here. The developed methodology of switching a relatively unstable motif within a biomacromolecule to a stable elemental isotopic mass signal on ICP-MS should find more applications when quantitative information on the linkage-specific motifs within a biomacromolecule or on the cell surface is mandatorily required for the elucidations of its distinct roles and understanding the pathological mechanisms, thus contributing to a more accurate diagnosis. More importantly, such quantitative breakdown information on the linkage-specific motifs within the functional meaningful biomacromolecules on the cell surface has been ever more expected for the development of novel target-based inhibitory drugs and/or corresponding vaccines for targeted clinical treatment of cancer in the future.

Limitations of the study

In this study, we developed a single-cell quantitative breakdown methodology of fucosylation mediated by Ac4-FucAz metabolic incorporation and ALK_{101}-PEG2000-MS2-DOTA-Eu_{979} clickable tagging on a single-cell ICP-MS platform. The limitation is mainly on the correlation between the quantitative fucosylation information obtained on a single cell and their exactly biological implications that need the intensive collaboration of chemists and biologists in the future. It is also worthy of pointing out that, not limited to fucosylation and its linkage-specific motifs, a cellular action should be governed synergistically by all the glycosylation happened on the cell.

Investigation on more kinds of glycosylation should be carried out for a more comprehensively multidimensional evaluation of cellular behaviors that is ongoing in our laboratory right now.

Resource availability

Lead contact

Further information and requests for resources should be directed to and will be fulfilled by the lead contact, Qiuquan Wang (qqwang@xmu.edu.cn).

Materials availability

This study did not generate new unique reagents.

Data and code availability

This study did not generate any data sets.

METHODS

All methods can be found in the accompanying Transparent methods supplemental file.

SUPPLEMENTAL INFORMATION

Supplemental information can be found online at https://doi.org/10.1016/j.isci.2021.102397.

ACKNOWLEDGMENTS

This study was financially supported by the National Natural Science Foundation of China (21535007, 21874112, and 22074127). We thank the Foundation for Innovative Research Groups of the National Natural Science Foundation of China (21521004) and the Program for Changjiang Scholars and Innovative Research Team in University (PCSIRT, IRT13036) for partly financial support. We also thank Dr. Pingguo Liu in the Hepatobiliary Surgery Division of Xiamen University Affiliated Zhong Shan Hospital for providing us clinical tissue samples.

AUTHOR CONTRIBUTIONS

Conceptualization, Q.W., Z.L., and Y.L.; methodology, Q.W., Z.L., and Y.L.; investigation, Z.L. and Y.L.; writing – original draft, Z.L.; writing – review & editing, Z.L. and Q.W.; funding acquisition, Q.W.; resources, Z.L., Y.Z., and F.G.; supervision, Q.W., X.Y., and L.Y.

DECLARATION OF INTERESTS

The authors declare no competing interests.

Received: December 10, 2020
Revised: March 5, 2021
Accepted: April 2, 2021
Published: May 21, 2021

REFERENCES

Acs, A., Ozohanics, O., Vekey, K., Drahos, L., and Turiak, L. (2018). Distinguishing core and antenna fucosylated glycopeptides based on low-energy tandem mass spectra. Anal. Chem. *90*, 12776–12782.

Adamczyk, B., Tharmalingam, T., and Rudd, P.M. (2012). Glycans as cancer biomarkers. Biochim. Biophys. Acta *1820*, 1347–1353.

Alley, W.R., Jr., Mann, B.F., and Novotny, M.V. (2013). High-sensitivity analytical approaches for the structural characterization of glycoproteins. Chem. Rev. *113*, 2668–2732.

Altschuler, S.J., and Wu, L.F. (2010). Cellular heterogeneity: do differences make a difference? Cell *141*, 559–563.

Aoyagi, Y., Suzuki, Y., Igarashi, K., Saitoh, A., Oguro, M., Yokota, T., Mori, S., Nomoto, M., Isemura, M., and Asakura, H. (1991). The usefulness of simultaneous determinations of glucosaminylation and fucosylation indices of alpha-fetoprotein in the differential diagnosis of neoplastic diseases of the liver. Cancer *67*, 2390–2394.

Bandura, D.R., Baranov, V.I., Ornatsky, O.I., Antonov, A., Kinach, R., Lou, X., Pavlov, S., Vorobiev, S., Dick, J.E., and Tanner, S.D. (2009). Mass cytometry: technique for real time single cell multitarget immunoassay based on inductively coupled plasma time-of-flight mass spectrometry. Anal. Chem. *81*, 6813–6822.

Barkeer, S., Chugh, S., Batra, S.K., and Ponnusamy, M.P. (2018). Glycosylation of cancer stem cells: function in stemness, tumorigenesis, and metastasis. Neoplasia *20*, 813–825.

Barthel, S.R., Wiese, G.K., Cho, J., Opperman, M.J., Hays, D.L., Siddiqui, J., Pienta, K.J., Furie, B., and Dimitroff, C.J. (2009). Alpha 1,3 fucosyltransferases are master regulators of prostate cancer cell trafficking. Proc. Natl. Acad. Sci. U S A *106*, 19491–19496.

Belo, A.I., van Vliet, S.J., Maus, A., Laan, L.C., Nauta, T.D., Koolwijk, P., Tefsen, B., and van Die, I. (2015). Hypoxia inducible factor 1α down regulates cell surface expression of α1,2-

fucosylated glycans in human pancreatic adenocarcinoma cells. FEBS Lett. *589*, 2359–2366.

Bendall, S.C., Simonds, E.F., Qiu, P., Amir el, A.D., Krutzik, P.O., Finck, R., Bruggner, R.V., Melamed, R., Trejo, A., Ornatsky, O.I., et al. (2011). Single-cell mass cytometry of differential immune and drug responses across a human hematopoietic continuum. Science *332*, 687–696.

Besanceney-Webler, C., Jiang, H., Zheng, T., Feng, L., Soriano del Amo, D., Wang, W., Klivansky, L.M., Marlow, F.L., Liu, Y., and Wu, P. (2011). Increasing the efficacy of bioorthogonal click reactions for bioconjugation: a comparative study. Angew. Chem. Int. Ed. *50*, 8051–8056.

Burkart, M.D., Vincent, S.P., Duffels, A., Murray, B.W., Ley, S.V., and Wong, C.H. (2000). Chemo-enzymatic synthesis of fluorinated sugar nucleotide: useful mechanistic probes for glycosyltransferases. Bioorg. Med. Chem. *8*, 1937–1946.

Cecioni, S., Imberty, A., and Vidal, S. (2015). Glycomimetics versus multivalent glycoconjugates for the design of high affinity lectin ligands. Chem. Rev. *115*, 525–561.

Chaubard, J.L., Krishnamurthy, C., Yi, W., Smith, D.F., and Hsieh-Wilson, L.C. (2012). Chemoenzymatic probes for detecting and imaging fucose-alpha(1-2)-galactose glycan biomarkers. J. Am. Chem. Soc. *134*, 4489–4492.

Chen, C.Y., Jan, Y.H., Juan, Y.H., Yang, C.J., Huang, M.S., Yu, C.J., Yang, P.C., Hsiao, M., Hsu, T.L., and Wong, C.H. (2013). Fucosyltransferase 8 as a functional regulator of nonsmall cell lung cancer. Proc. Natl. Acad. Sci. U S A *110*, 630–635.

Fukushima, K., Satoh, T., Baba, S., and Yamashita, K. (2009). α1,2-Fucosylated and β-N-acetylgalactosaminylated prostate-specific antigen as an efficient marker of prostatic cancer. Glycobiology *20*, 452–460.

Ghazarian, H., Idoni, B., and Oppenheimer, S.B. (2011). A glycobiology review: carbohydrates, lectins and implications in cancer therapeutics. Acta Histochem. *113*, 236–247.

Gotz, L., Abrahams, J.L., Mariethoz, J., Rudd, P.M., Karlsson, N.G., Packer, N.H., Campbell, M.P., and Lisacek, F. (2014). GlycoDigest: a tool for the targeted use of exoglycosidase digestions in glycan structure determination. Bioinformatics *30*, 3131–3133.

Harvey, D.J., Mattu, T.S., Wormald, M.R., Royle, L., Dwek, R.A., and Rudd, P.M. (2002). "Internal residue loss": rearrangements occurring during the fragmentation of carbohydrates derivatized at the reducing terminus. Anal. Chem. *74*, 734–740.

Hsu, T.L., Hanson, S.R., Kishikawa, K., Wang, S.K., Sawa, M., and Wong, C.H. (2007). Alkynyl sugar analogs for the labeling and visualization of glycoconjugates in cells. Proc. Natl. Acad. Sci. U S A *104*, 2614–2619.

Lattova, E., Skrickova, J., and Zdrahal, Z. (2019). Applicability of phenylhydrazine labeling for structural studies of fucosylated N-glycans. Anal. Chem. *91*, 7985–7990.

Laughlin, S.T., and Bertozzi, C.R. (2007). Metabolic labeling of glycans with azido sugars and subsequent glycan-profiling and visualization via Staudinger ligation. Nat. Protoc. *2*, 2930–2944.

Li, F., Armstrong, D.W., and Houk, R.S. (2005). Behavior of bacteria in the inductively coupled plasma: atomization and production of atomic ions for mass spectrometry. Anal. Chem. *77*, 1407–1413.

Li, J., Hsu, H.C., Mountz, J.D., and Allen, J.G. (2018). Unmasking fucosylation: from cell adhesion to immune system regulation and diseases. Cell Chem. Biol. *25*, 499–512.

Liang, Y., Yang, L., and Wang, Q. (2015). An ongoing path of element-labeling/tagging strategies toward quantitative bioanalysis using ICP-MS. Appl. Spectrosc. Rev. *51*, 117–128.

Lis, H., and Sharon, N. (1998). Lectins: carbohydrate-specific proteins that mediate cellular recognition. Chem. Rev. *98*, 637–674.

Liu, R., Zhang, S., Wei, C., Xing, Z., Zhang, S., and Zhang, X. (2016). Metal stable isotope tagging: renaissance of radioimmunoassay for multiplex and absolute quantification of biomolecules. Acc. Chem. Res. *49*, 775–783.

Luo, Y., Yan, X., Huang, Y., Wen, R., Li, Z., Yang, L., Yang, C.J., and Wang, Q. (2013). ICP-MS-based multiplex and ultrasensitive assay of viruses with lanthanide-coded biospecific tagging and amplification strategies. Anal. Chem. *85*, 9428–9432.

Ma, B., Simala-Grant, J.L., and Taylor, D.E. (2006). Fucosylation in prokaryotes and eukaryotes. Glycobiology *16*, 158–184.

Marionneau, S., Cailleau-Thomas, A., Rocher, J., Le Moullac-Vaidye, B., Ruvoën, N., Clément, M., and Le Pendu, J. (2001). ABH and Lewis histo-blood group antigens, a model for the meaning of oligosaccharide diversity in the face of a changing world. Biochimie *83*, 565–573.

Mathieu, S., Prorok, M., Benoliel, A.-M., Uch, R., Langlet, C., Bongrand, P., Gerolami, R., and El-Battari, A. (2004). Transgene expression of α(1,2)-fucosyltransferase-I (FUT1) in tumor cells selectively inhibits sialyl-lewis x expression and binding to E-selectin without affecting synthesis of sialyl-lewis a or binding to P-selectin. Am. J. Pathol. *164*, 371–383.

Montaser, A. (1998). Inductively Coupled Plasma Mass Spectrometry (Wiley).

Moriwaki, K., and Miyoshi, E. (2010). Fucosylation and gastrointestinal cancer. World J. Hepatol. *2*, 151–161.

Noda, K., Miyoshi, E., Gu, J.G., Gao, C.X., Nakahara, S., Kitada, T., Honke, K., Suzuki, K., Yoshihara, H., Yoshikawa, K., et al. (2003). Relationship between elevated FX expression and increased production of GDP-L-fucose, a common donor substrate for fucosylation in human hepatocellular carcinoma and hepatoma cell lines. Cancer Res. *63*, 6282–6289.

Nwosu, C., Yau, H.K., and Becht, S. (2015). Assignment of core versus antenna fucosylation types in protein N-glycosylation via procainamide labeling and tandem mass spectrometry. Anal. Chem. *87*, 5905–5913.

Ohtsubo, K., and Marth, J.D. (2006). Glycosylation in cellular mechanisms of health and disease. Cell *126*, 855–867.

Palaniappan, K.K., and Bertozzi, C.R. (2016). Chemical glycoproteomics. Chem. Rev. *116*, 14277–14306.

Pelkmans, L. (2012). Using cell-to-cell variability-A new era in molecular biology. Science *336*, 425–426.

Pinho, S.S., and Reis, C.A. (2015). Glycosylation in cancer: mechanisms and clinical implications. Nat. Rev. Cancer *15*, 540–555.

Rabuka, D., Hubbard, S.C., Laughlin, S.T., Argade, S.P., and Bertozzi, C.R. (2006). A chemical reporter strategy to probe glycoprotein fucosylation. J. Am. Chem. Soc. *128*, 12078–12079.

Ruhaak, L.R., Xu, G., Li, Q., Goonatilleke, E., and Lebrilla, C.B. (2018). Mass spectrometry approaches to glycomic and glycoproteomic analyses. Chem. Rev. *118*, 7886–7930.

Sanz-Medel, A., Montes-Bayón, M., Bettmer, J., Luisa Fernández-Sanchez, M., and Ruiz Encinar, J. (2012). ICP-MS for absolute quantification of proteins for heteroatom-tagged, targeted proteomics. Trend Anal. Chem. *40*, 52–63.

Sawa, M., Hsu, T.L., Itoh, T., Sugiyama, M., Hanson, S.R., Vogt, P.K., and Wong, C.H. (2006). Glycoproteomic probes for fluorescent imaging of fucosylated glycans in vivo. Proc. Natl. Acad. Sci. U S A *103*, 12371–12376.

Schneider, M., Al-Shareffi, E., and Haltiwanger, R.S. (2017). Biological functions of fucose in mammals. Glycobiology *27*, 601–618.

Taylor, P., Takeuchi, H., Sheppard, D., Chillakuri, C., Lea, S.M., Haltiwanger, R.S., and Handford, P.A. (2014). Fringe-mediated extension of O-linked fucose in the ligand-binding region of Notch1 increases binding to mammalian Notch ligands. Proc. Natl. Acad. Sci. U S A *111*, 7290–7295.

Teichmann, S. (2019). Expand single-cell biology. Nature *565*, 521–522.

Uttamapinant, C., Tangpeerachaikul, A., Grecian, S., Clarke, S., Singh, U., Slade, P., Gee, K.R., and Ting, A.Y. (2012). Fast, cell-compatible click chemistry with copper-chelating azides for biomolecular labeling. Angew. Chem. Int. Ed. *51*, 5852–5856.

Virani, F., and Tanner, S.D. (2015). Mass cytometry: an evolution in ICP-ms enabling novel insights in single-cell biology. Spectroscopy *30*, 14–22.

Wald, C., Russo, M.W., Heimbach, J.K., Hussain, H.K., Pomfret, E.A., and Bruix, J. (2013). New OPTN/UNOS policy for liver transplant allocation: standardization of liver imaging, diagnosis, classification, and reporting of hepatocellular carcinoma. Radiology *266*, 376–382.

Wang, Y., Fukuda, T., Isaji, T., Lu, J., Im, S., Hang, Q., Gu, W., Hou, S., Ohtsubo, K., and Gu, J. (2015). Loss of alpha1,6-fucosyltransferase inhibits chemical-induced hepatocellular carcinoma and tumorigenesis by down-regulating several cell signaling pathways. FASEB J. *29*, 3217–3227.

Wei, X., Lu, Y., Zhang, X., Chen, M.L., and Wang, J.H. (2020). Recent advances in single-cell ultra-trace analysis. Trend Anal. Chem. *127*, 115886–115908.

Yan, X., Xu, M., Yang, L., and Wang, Q. (2010). Absolute quantification of intact proteins via 1,4,7,10-Tetraazacyclododecane-1,4,7-trisacetic acid−10-Maleimidoethylacetamide−Europium labeling and HPLC coupled with species-unspecific isotope dilution ICPMS. Anal. Chem. *82*, 1261–1269.

Yan, X., Yang, L., and Wang, Q. (2011). Lanthanide-coded protease-specific peptide-nanoparticle probes for a label-free multiplex protease assay using element mass spectrometry: a proof-of-concept study. Angew. Chem. Int. Ed. *50*, 5130–5133.

Yan, X., Yang, L., and Wang, Q. (2013). Detection and quantification of proteins and cells by use of elemental mass spectrometry: progress and challenges. Anal. Bioanal. Chem. *405*, 5663–5670.

Yan, S., Vanbeselaere, J., Jin, C., Blaukopf, M., Wöls, F., Wilson, I.B.H., and Paschinger, K. (2018). Core richness of N-glycans of Caenorhabditis elegans: a case study on chemical and enzymatic release. Anal. Chem. *90*, 928–935.

Yin, X., Rana, K., Ponmudi, V., and King, M.R. (2010). Knockdown of fucosyltransferase III disrupts the adhesion of circulating cancer cells to E-selectin without affecting hematopoietic cell adhesion. Carbohyd. Res. *345*, 2334–2342.

Yuan, R., Ge, F., Liang, Y., Zhou, Y., Yang, L., and Wang, Q. (2019a). Viruslike element-tagged nanoparticle inductively coupled plasma mass spectrometry signal multiplier: membrane biomarker mediated cell counting. Anal. Chem. *91*, 4948–4952.

Yuan, W., Wei, R., Goldman, R., and Sanda, M. (2019b). Optimized fragmentation for quantitative analysis of fucosylated N-glycoproteins by LC-MS-MRM. Anal. Chem. *91*, 9206–9212.

Zhou, Y., Chen, Z., Zeng, J., Zhang, J., Yu, D., Zhang, B., Yan, X., Yang, L., and Wang, Q. (2020). Direct infusion ICP-qMS of lined-up single-cell using an oil-free passive microfluidic system. Anal. Chem. *92*, 5286–5293.

iScience, Volume *24*

Supplemental information

Single-cell fucosylation breakdown:

Switching fucose to europium

Zhen Liu, Yong Liang, Yang Zhou, Fuchun Ge, Xiaowen Yan, Limin Yang, and Qiuquan Wang

Supplemental Information

Supplemental Schemes and Legends

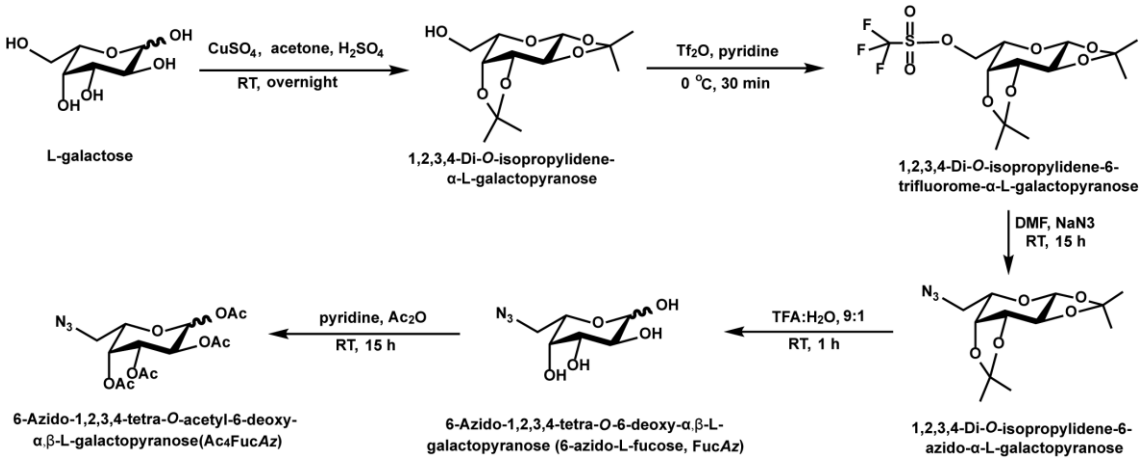

Scheme S1. Synthetic routes of Ac_4Fuc*Az*. (Related to Scheme 1)

Supplemental Figures and Legends

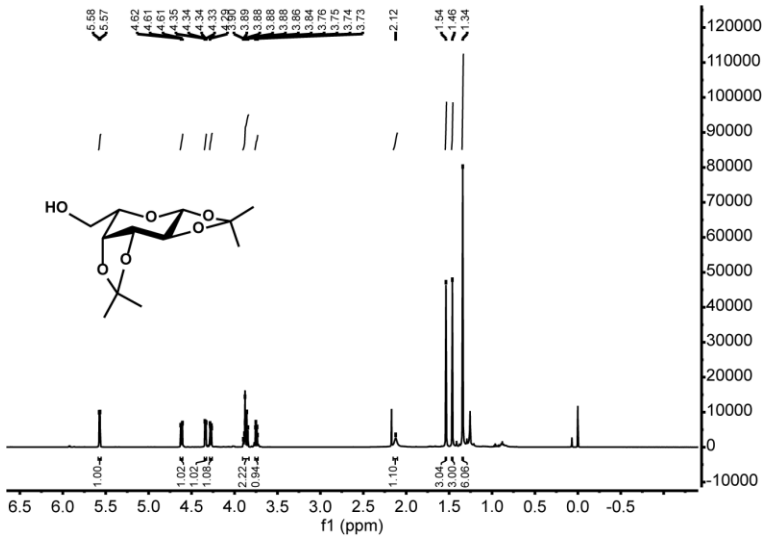

Figure S1. ^{1}HNMR spectrum of 1,2,3,4-Di-*O*-isopropylidene-α-L-galactopyranose ((500 MHz, $CDCl_3$), δ 5.57 (d, *J* = 5.0 Hz, 1H), 4.62 (dd, *J* = 7.9, 2.4 Hz, 1H), 4.34 (dd, *J* = 5.0, 2.4 Hz, 1H), 4.28 (dd, *J* = 7.9, 1.5 Hz, 1H), 3.90-3.83 (m, 2H), 3.74 (dd, 1H), 2.12 (s, 2H), 1.54 (s, 3H), 1.46 (s, 3H), 1.34 (s, 6H)). (Related to Scheme 1)

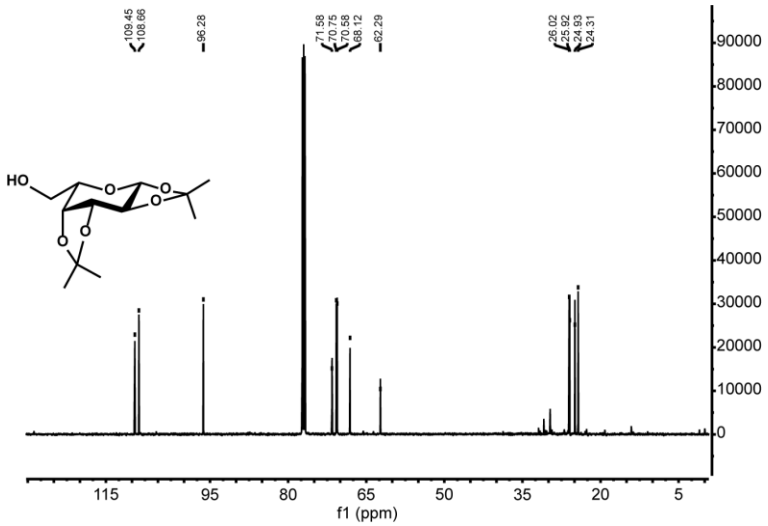

Figure S2. ^{13}CNMR spectrum of 1,2,3,4-Di-*O*-isopropylidene-α-L-galactopyranose ((126 MHz, $CDCl_3$), δ 109.45, 108.66, 96.28, 71.58, 70.75, 70.58, 68.12, 62.29, 26.02, 25.92, 24.93, 24.31). (Related to Scheme 1)

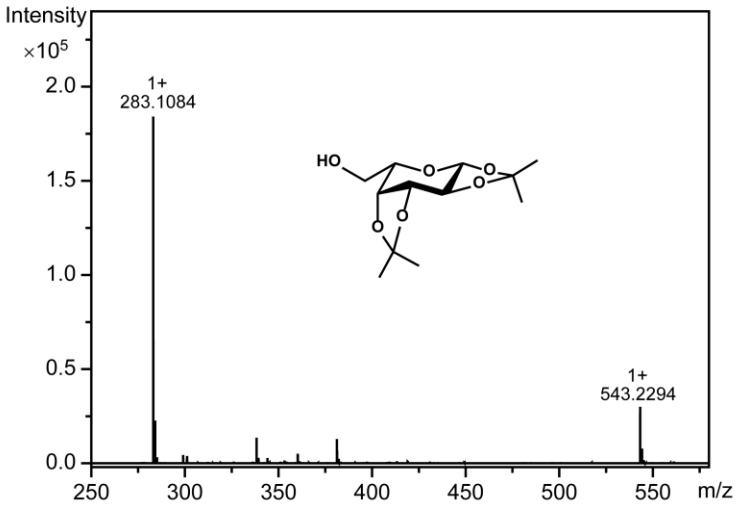

Figure S3. ESI-*q*TOF-MS spectrum of 1,2,3,4-Di-*O*-isopropylidene-α-L-galactopyranose (calcd. $C_{12}H_{20}O_6$: m/z 260.1260, found $[M+Na]^+$ 283.1084; $[2M+Na]^+$ 543.2294). (Related to Scheme 1)

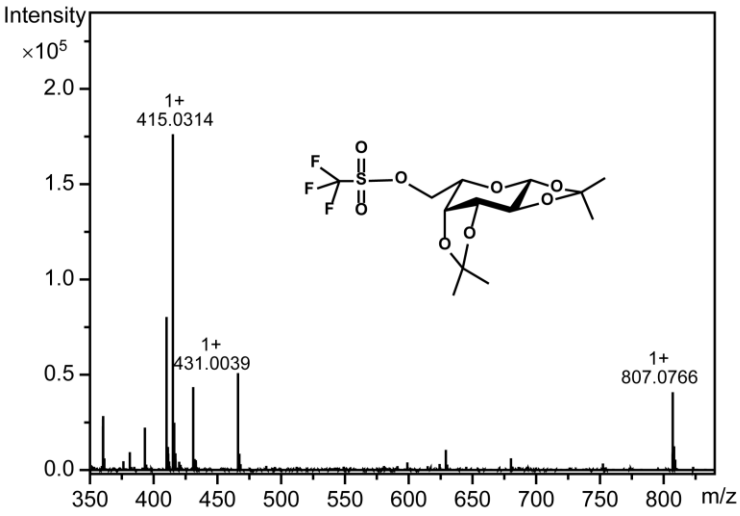

Figure S4. ESI-*q*TOF-MS spectrum of 1,2,3,4-Di-*O*-isopropylidene-6-trifluorome-α-L-galactopyranose (calcd. $C_{13}H_{19}F_3O_8S$: m/z 392.0753, found $[M+Na]^+$ 415.0314; $[M+K]^+$ 431.0039; $[2M+Na]^+$ 807.0766). (Related to Scheme 1)

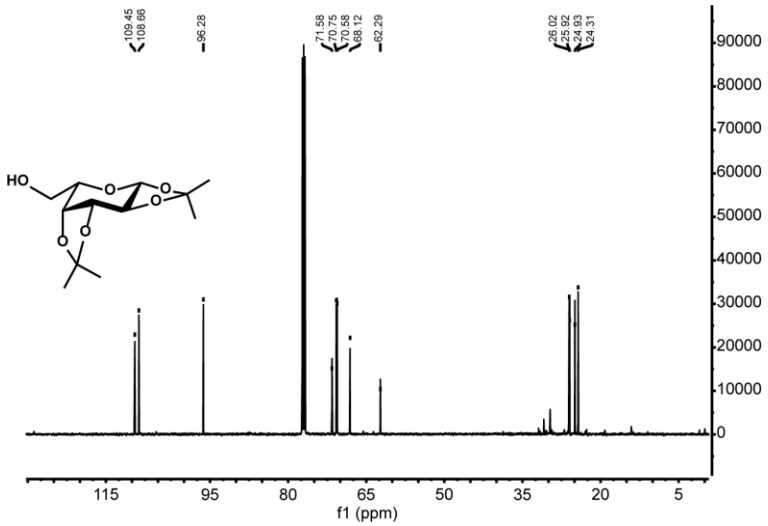

Figure S5. ^{1}HNMR spectrum of 1,2,3,4-Di-*O*-isopropylidene-6-azido-α-L-galactopyranose ((500 MHz, $CDCl_3$) δ 5.48 (d, *J* = 5.0 Hz, 1H), 4.56 (dd, *J* = 7.8, 2.5 Hz, 1H), 4.26 (dd, *J* = 5.0, 2.4 Hz, 1H), 4.12 (dd, *J* = 7.9, 2.0 Hz, 1H), 3.91-3.76 (m, 1H), 3.44 (dd, *J* = 12.7, 7.8 Hz, 1H), 3.29 (dd, *J* = 12.7, 5.4 Hz, 1H), 1.48 (s, 3H), 1.39 (s, 3H), 1.26 (s, 6H)). (Related to Scheme 1)

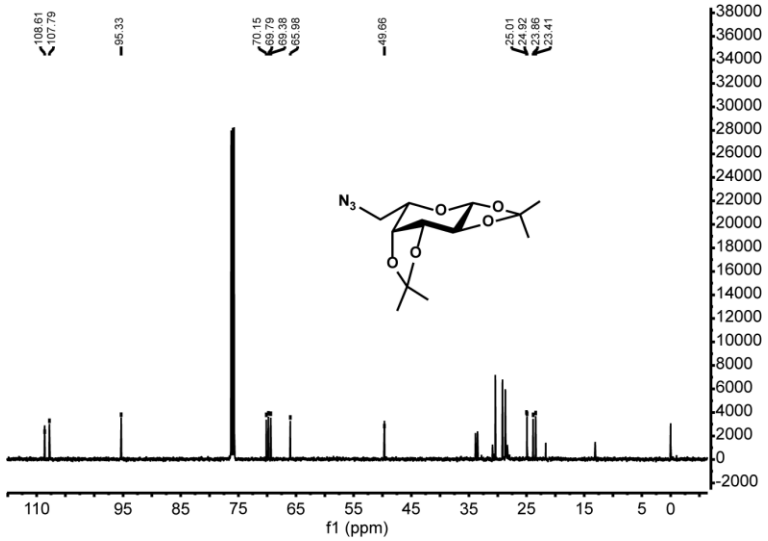

Figure S6. ^{13}CNMR spectrum of 1,2,3,4-Di-*O*-isopropylidene-6-azido-α-L-galactopyranose ((126 MHz, $CDCl_3$) δ 108.61, 107.79, 95.33, 70.15, 69.79, 69.38, 65.98, 49.66, 25.01, 24.92, 23.86, 23.41). (Related to Scheme 1)

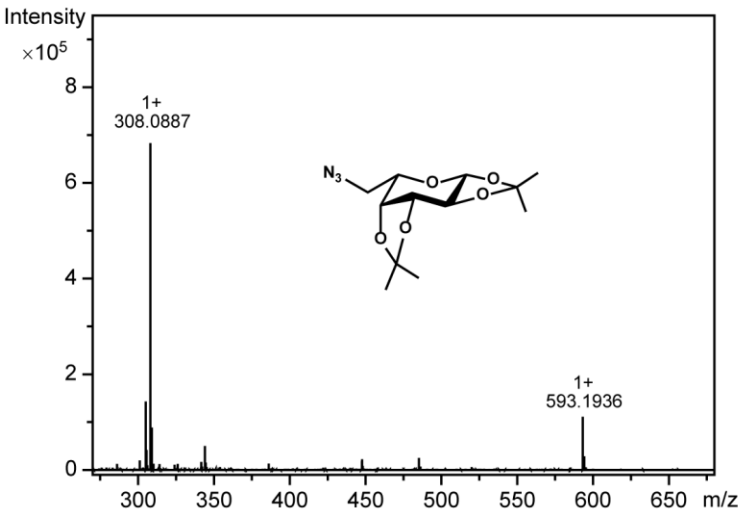

Figure S7. ESI-*q*TOF-MS spectrum of 1,2,3,4-Di-*O*-isopropylidene-6-azido-α-L-galactopyranose (calcd. $C_{12}H_{19}N_3O_5$: m/z 285.1325, found $[M+Na]^+$ 308.0887; $[2M+Na]^+$ 593.1936). (Related to Scheme 1)

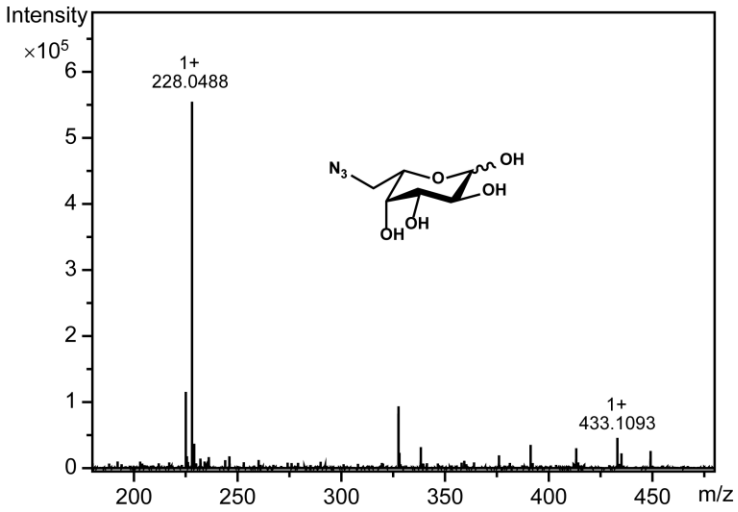

Figure S8. ESI-*q*TOF-MS spectrum of 6-azido-1,2,3,4-tetra-*O*-6-deoxy-α,β-L-galactopyranose (calcd. $C_6H_{11}N_3O_5$: m/z 205.0699, found $[M+Na]^+$ 228.0488; $[2M+Na]^+$ 433.1093). (Related to Scheme 1)

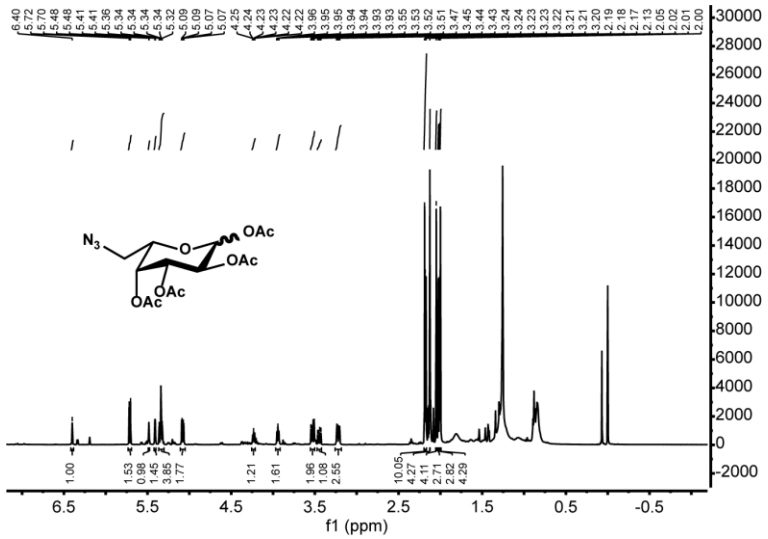

Figure S9. ^{1}HNMR spectrum of 6-azido-1,2,3,4-tetra-*O*-acetyl-6-deoxy-α,β-L-galactopyranose ((500 MHz, $CDCl_3$) δ 6.40 (s, H-1α), 5.71 (d, *J* = 8.3 Hz, H-1β), 5.48 (d, *J* = 1.4 Hz), 5.41 (d, *J* = 3.3 Hz), 5.37-5.30 (m), 5.08 (dd, *J* = 10.4, 3.4 Hz), 4.26-4.19 (m, H-5α), 3.96-3.92 (m, H-5β), 3.53 (dd, *J* = 12.9, 7.4 Hz), 3.45 (dd, *J* = 12.8, 7.4 Hz, 1H), 3.27-3.18 (m), 2.20-2.16 (m), 2.13 (s), 2.05 (s, 3H), 2.02 (s), 2.01 (s), 2.00 (s)). (Related to Scheme 1)

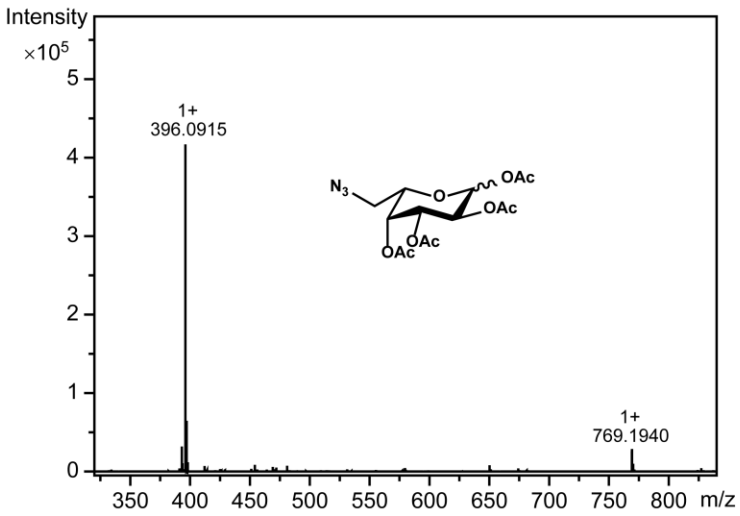

Figure S10. ESI-*q*TOF-MS spectrum of 6-azido-1,2,3,4-tetra-*O*-acetyl-6-deoxy-α,β-L-galactopyranose (calcd. $C_{14}H_{19}N_3O_9$: m/z 373.1121, found $[M+Na]^+$ 396.0915; $[2M+Na]^+$ 769.1940). (Related to Scheme 1)

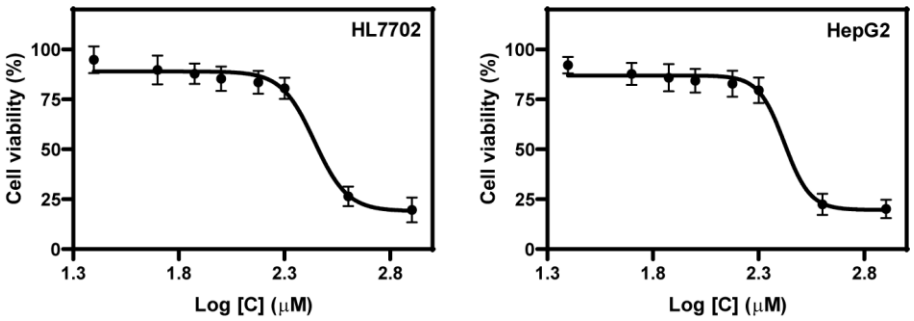

Figure S11. CCK-8 assay of cell viability after incubating with 0 to 800 μM Ac_4Fuc*Az*. Cells were plated in a 96-well microliter plate, seven parallel specimens (2.0×10^4 cell each) and cultured for 48 h. Afterwards, the cells were rinsed with PBS 5 times and then assayed using a standard cell counting kit-8 (CCK-8). The cell viability was determined at λ = 450 nm, and compared with the controls. The error bars indicate the standard deviation calculated from seven repetitive experiments results. (Related to Figure 2)

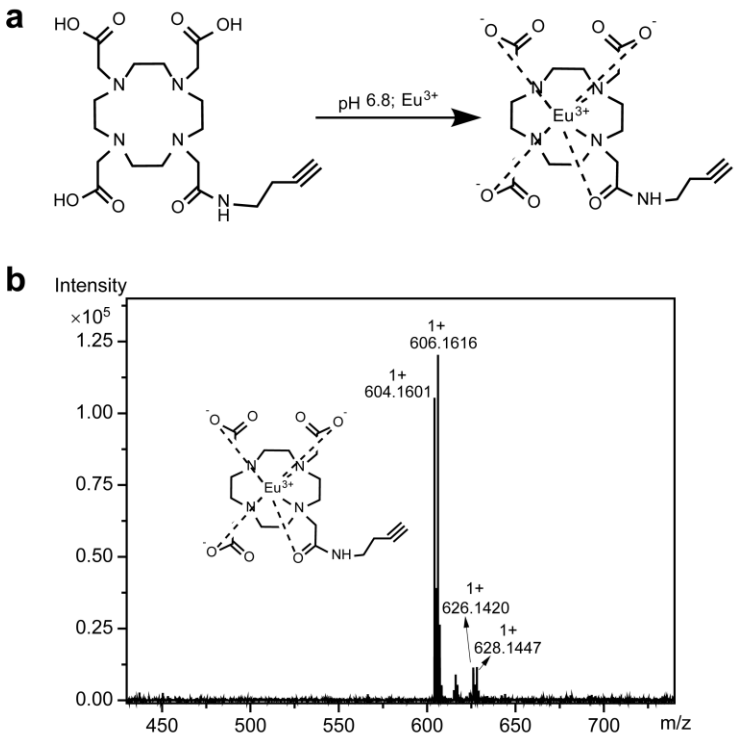

Figure S12. Synthetic route (a) and ESI-*q*TOF-MS (b) of *ALK*-DOTA-Eu. (calcd. $C_{20}H_{30}EuN_5O_7$: m/z 603.1344/605.1357, found $[M+H]^+$ 604.1601/606.1616, $[M+Na]^+$ 626.1420/628.1447). (Related to Scheme 1)

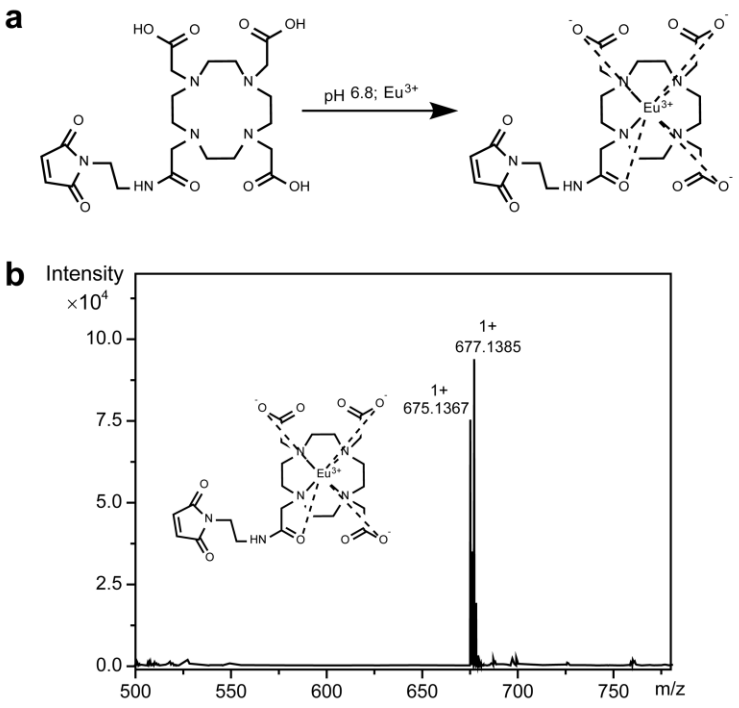

Figure S13. Synthetic route (a) and ESI-*q*TOF-MS (b) of *MAL*-DOTA-Eu (calcd. $C_{22}H_{31}EuN_6O_9$: m/z 674.1351/676.1365, found $[M+H]^+$ 675.1367/677.1385). (Related to Scheme 1)

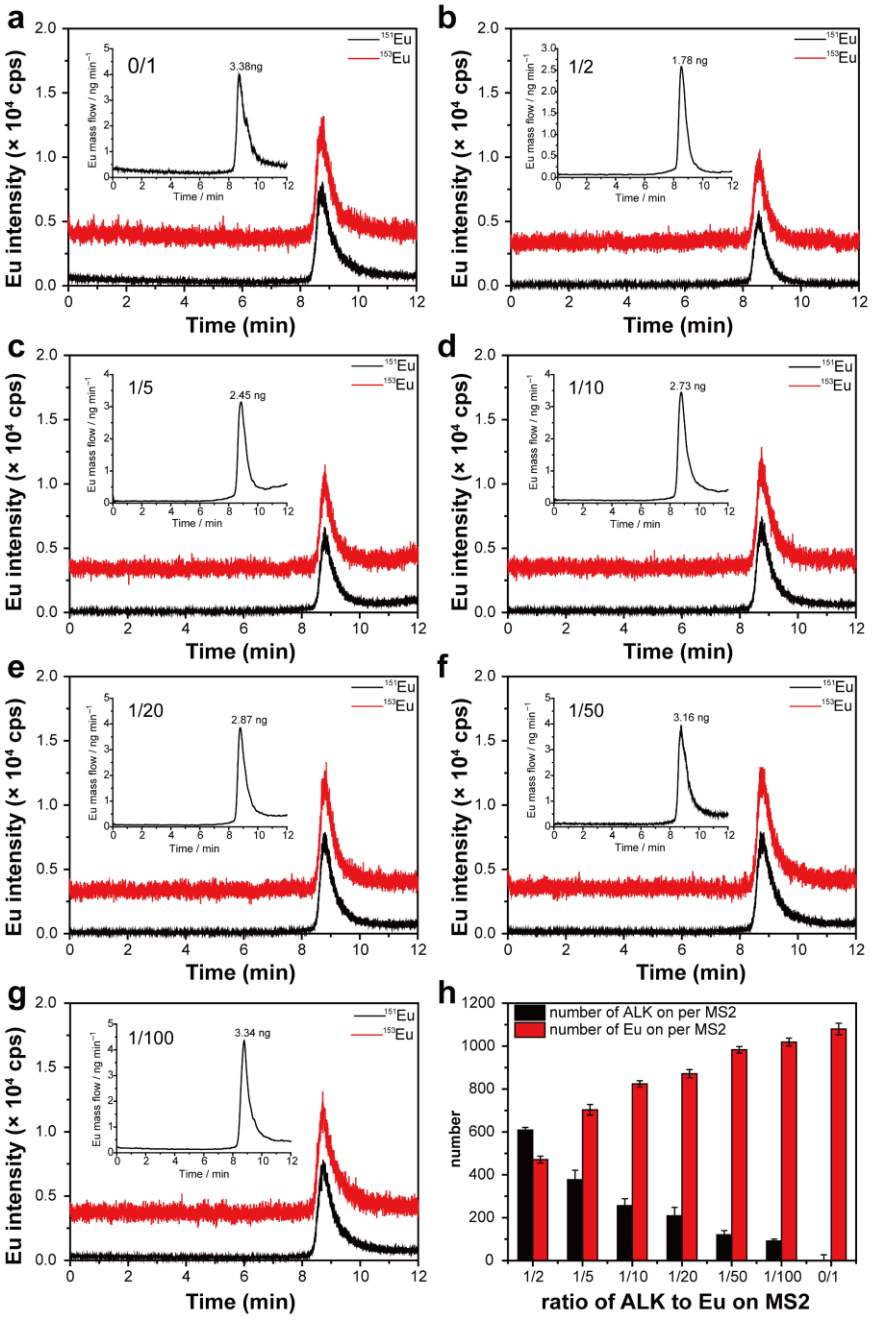

Figure S14. Characterization of *MAL*-PEG2000-*ALK* and *MAL*-DOTA-Eu modified MS2 at different ratios of 0/1, 1/2, 1/5, 1/10, 1/25, 1/50, 1/100 (a-g) and the number of *MAL*-PEG2000-*ALK* and *MAL*-DOTA-Eu on one MS2 capsid (h) evaluated by SEC-^{153}Eu-SUID-ICP-MS (n = 7). The insert graph was the Eu mass flow calculated from the isotope dilution equation. (Related to Figure 1)

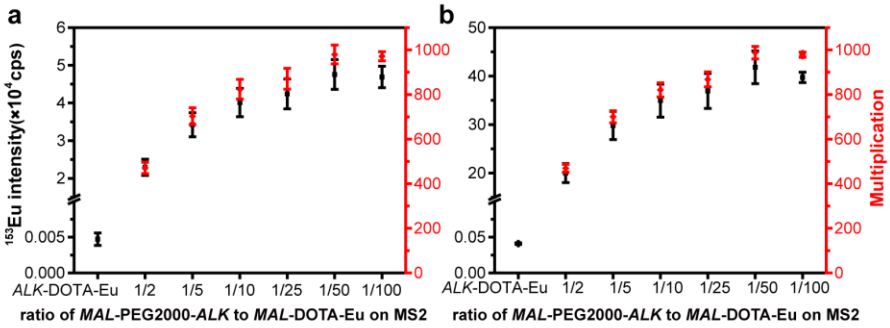

Figure S15. Signal-multiplication of *ALK*-PEG2000-MS2-DOTA-Eu prepared at different ratios of *MAL*-PEG2000-*ALK* to *MAL*-DOTA-Eu at 1/2, 1/5, 1/10, 1/25, 1/50, and 1/100 regarding the tagged Fuc*Az* on the cell-surface of HL7702 (a) and HepG2 (b) and determined using ^{153}Eu-SUID-ICP-MS (n = 7). 2.5 × 10^4 cells/mL were employed. (Related to Figure 1)

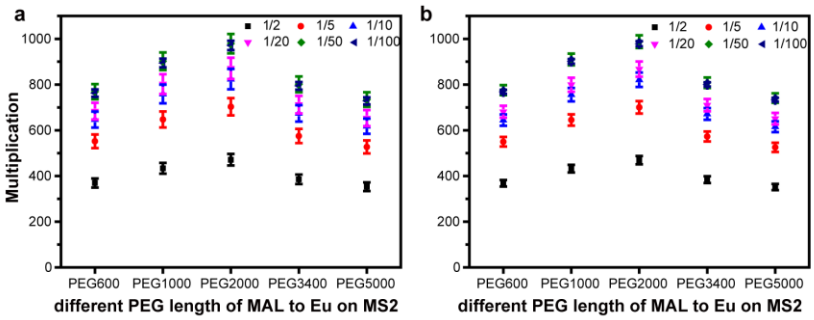

Figure S16. Signal multiplication of *ALK*-PEG-MS2-DOTA-Eu prepared using different length PEG (PEG600, PEG1000, PEG2000, PEG3400 and PEG5000) under different ratios of *MAL*-PEG-*ALK* to *MAL*-DOTA-Eu at 1/2, 1/5, 1/10, 1/25, 1/50, and 1/100, which tagged to Fuc*Az* on the cell-surface of HL7702 (a) and HepG2 (b) and determined using ^{153}Eu-SUID-ICPMS (n = 7). 2.5 × 10^4 cells/mL were employed. (Related to Figure 1)

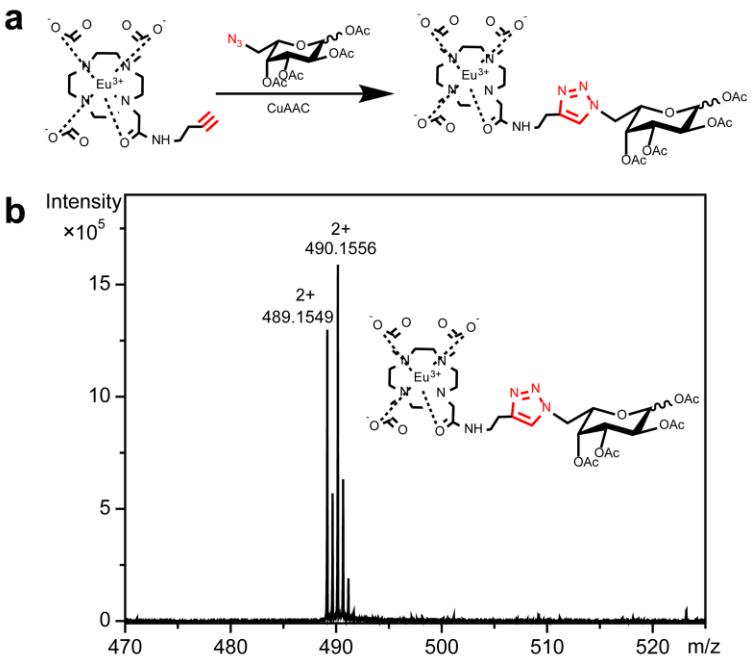

Figure S17. Synthetic route (a) and ESI-*q*TOF-MS (b) of Fuc*Az*-*ALK*-DOTA-Eu with 1:1 stoichiometry between azide and alkyne group (calcd. $C_{34}H_{49}EuN_8O_{16}$: m/z 976.2465/978.2479, found $[M+H]^{2+}$ 489.1549/490.1556). (Related to Figure 1)

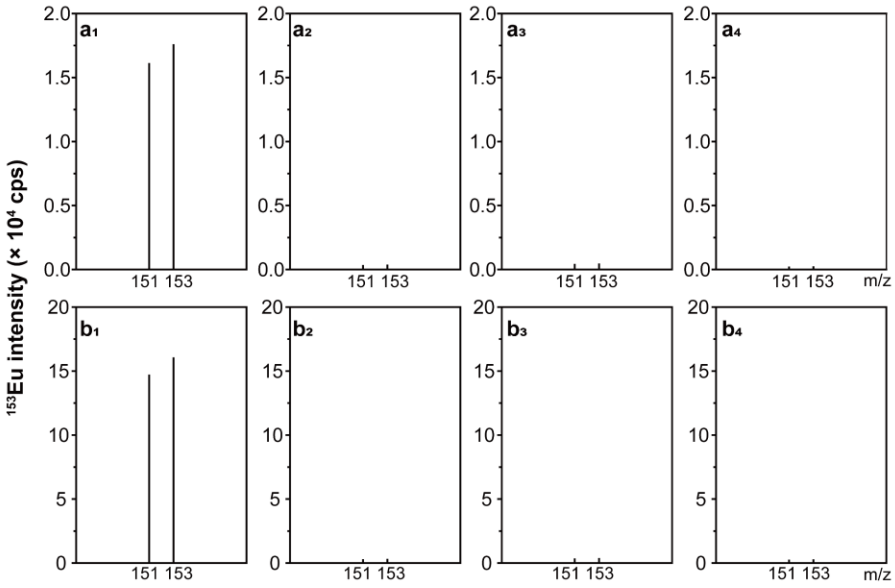

Figure S18. $^{151/153}$Eu-signal of *ALK*-DOTA-Eu tagged Fuc*Az* on the cell-surface of HL7702 (a) and HepG2 (b) (1.0 × 10^6 cells/mL) on ICP-MS. (a_1, b_1) with Ac_4Fuc*Az* cultivation and *ALK*-DOTA-Eu tagging via CuAAC; (a_2, b_2) with *ALK*-DOTA-Eu tagging but without Ac_4Fuc*Az* cultivation; (a_3, b_3) with Ac_4Fuc*Az* cultivation but without *ALK*-DOTA-Eu tagging; (a_4, b_4) without Ac_4Fuc*Az* cultivation and *ALK*-DOTA-Eu tagging. (Related to Figure 2)

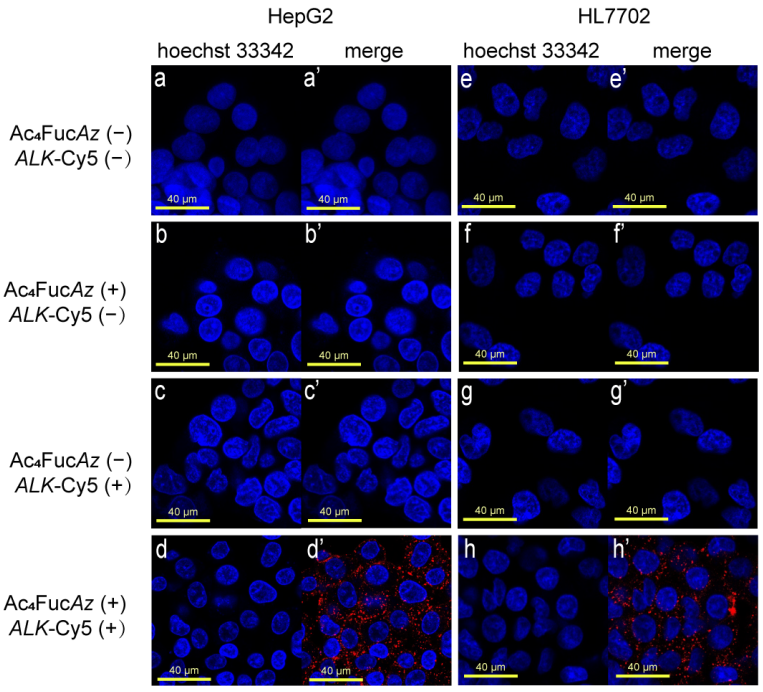

Figure S19. Fluorescence micrographs of the cell-surface Fuc*Az* of HepG2 and HL7702 labeled by *ALK*-Cy5. Cells treated with 200 μM Ac_4Fuc*Az* for 48 h and then rinsed, after that the cells were subjected to the fluorescence labeling procedure. (a, a', e, e') without Ac_4Fuc*Az* cultivation and *ALK*-Cy5 labeling via CuAAC; (b, b', f, f') with Ac_4Fuc*Az* cultivation but without *ALK*-Cy5 labeling; (c, c', g, g') with *ALK*-Cy5 labeling but without Ac_4Fuc*Az* cultivation; (d, d', h, h') with Ac_4Fuc*Az* cultivation and *ALK*-Cy5 labeling. Blue fluorescence, stained with hoechst 33342 for nuclei; Red fluorescence, labeled with *ALK*-Cy5 for Fuc*Az*. Scale bars = 40 μm**.** (Related to Figure 2)

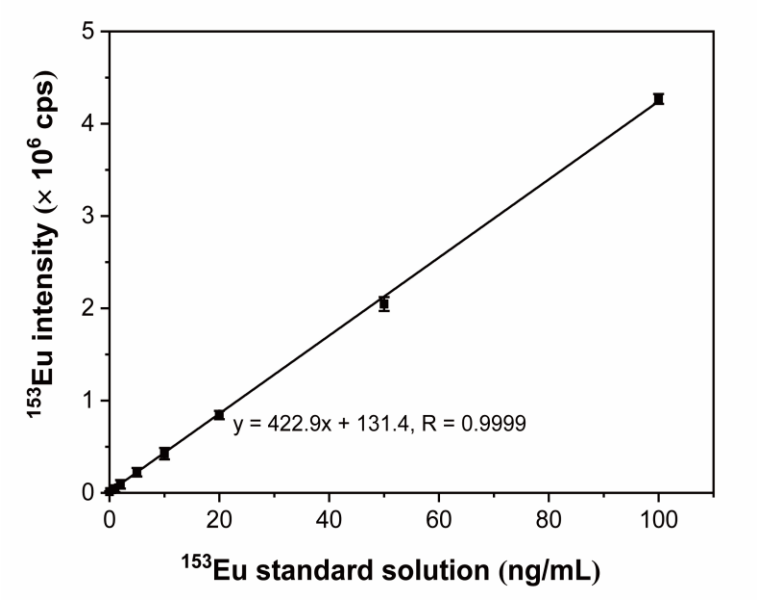

Figure S20. Calibration curve constructed by ^{153}Eu standard solution of 0, 1, 2, 5, 10, 20, 50 and 100 ng/mL, respectively, against ^{153}Eu-signal intensity on the single-cell ICP-MS platform with the dwell time of 10 ms. (Related to Figure 2)

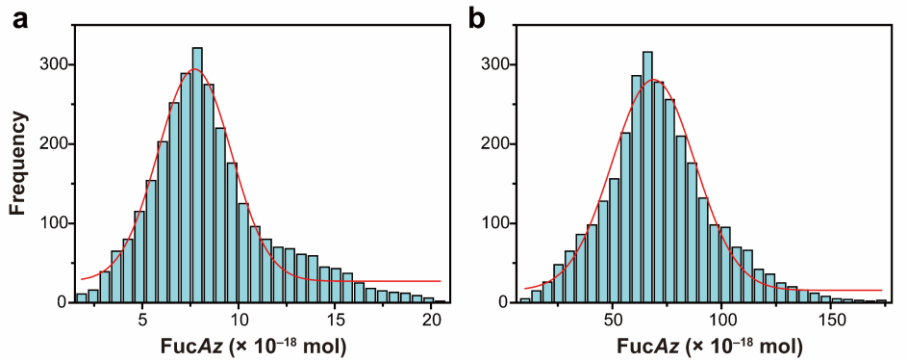

Figure S21. Gaussian fitting of the single cell events of HL7702 (a) and HepG2 (b) cells tagged with *ALK*$_{101}$-PEG2000-MS2-DOTA-Eu$_{979}$ based on the total Fuc*Az* content on the single cell versus frequency of single-cell events on the single-cell ICP-MS platform statistically counted from 3000-independent valid single-cell events. (Related to Figure 2)

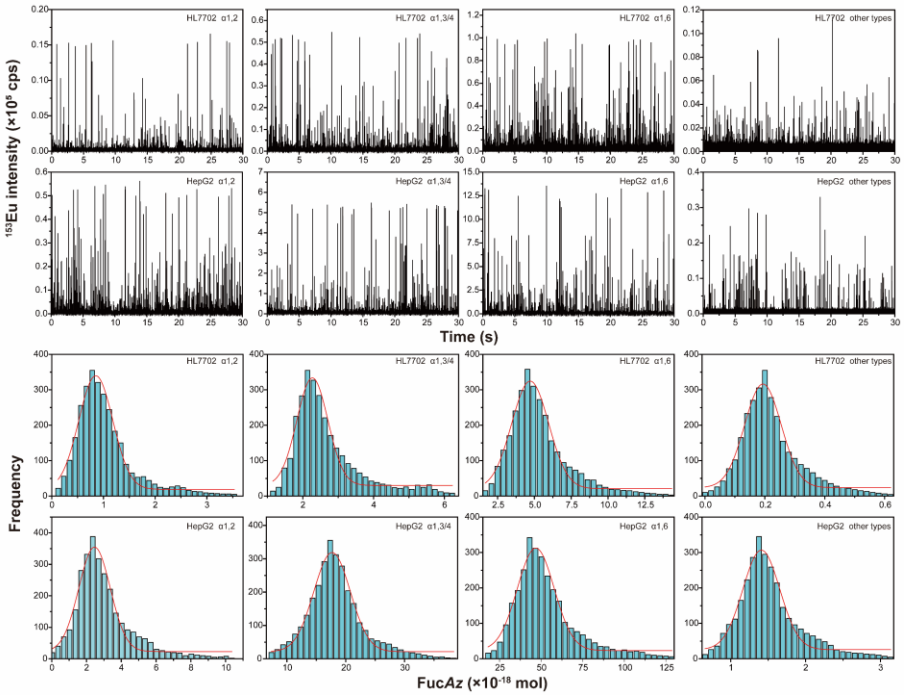

Figure S22. Single cell events and Gaussian fitting of different Fuc*Az* linkage-specific motifs including α1,2, α1,3/4, α1,6 and other types on HL7702 and HepG2 cells tagged with ALK_{101}-PEG2000-MS2-DOTA-Eu_{979} based on their corresponding contents determined on the single cell versus frequency of single-cell events on the single-cell ICP-MS platform. (Related to Figure 3)

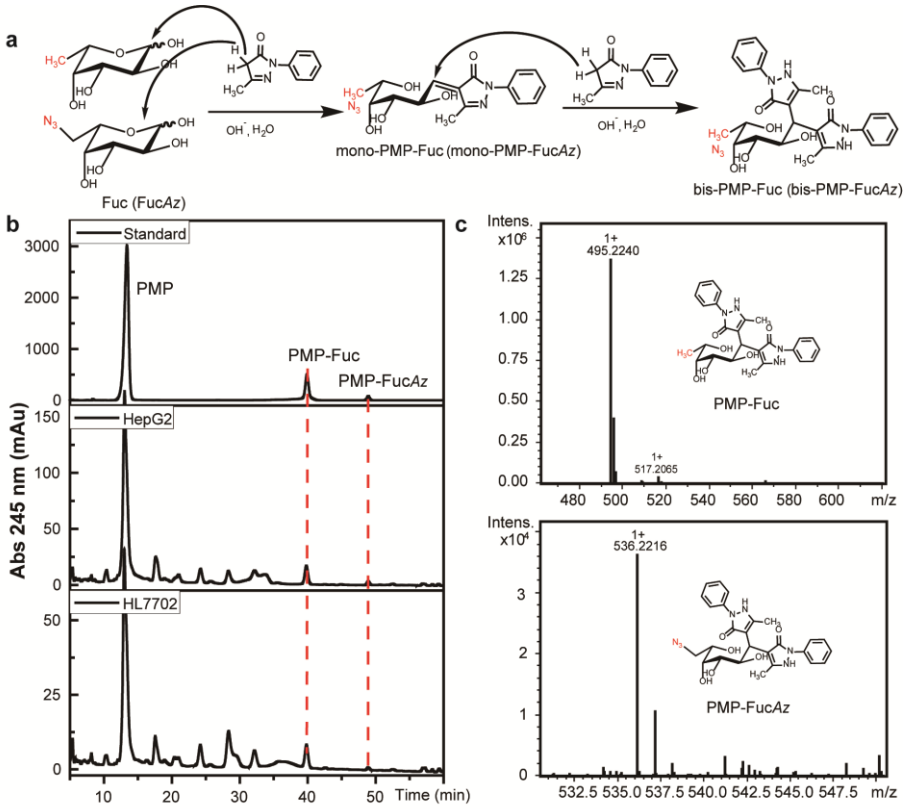

Figure S23. Fuc and Fuc*Az* on the cell-surface of HepG2 and HL7702 cells detected by using PMP derivatization HPLC at 245 nm (n = 3). PMP derivatization (a); PMP-derivatized monosaccharide samples determined by HPLC, PMP-Fuc at 39.8 min and PMP-Fuc*Az* at 48.8 min (b); ESI-*q*TOF-MS of PMP-Fuc and PMP-Fuc*Az* (c) (calcd. PMP-Fuc, $C_{26}H_{30}N_4O_6$: m/z 494.2165, found $[M+H]^+$ 495.2240，$[M+Na]^+$ 517.2065; PMP-Fuc*Az*, $C_{26}H_{29}N_7O_6$: m/z 535.2179, found $[M+H]^+$ 536.2216). 1.0×10^7 cells of HepG2 and HL7702 each were used. (Related to Figure 2)

Supplemental Tables

Table S1. Average FucAz contents of the fucosidic linkage-specific motifs on the cells from the clinical tissues resected from the patients with normal hepatocellular tissue and variously differentiated HCC including highly, moderately and poorly differentiation HCC determined on the single-cell ICP-MS platform (n=5), and their corresponding pathological information. (Related to Figure 3)

tissues	Patient ID	α1,2	α1,3/4	α1,6	other	total	gender	age	Size[e]	Ki67[f]	AFP[g]	CEA[h]	CA125[i]	CA199[j]
normal	638794	6.3 ± 0.8[a]	3.7 ± 0.9[b]	1.1 ± 0.2[c]	1.5 ± 0.4[a]	1.6 ± 0.3[c]	M	58	15.4 x 11.3 x 3.6	*	4.49	2.89	7.39	14
	503897	1.3 ± 0.4[b]	4.4 ± 0.5[b]	8.6 ± 1.1[b]	2.8 ± 0.5[a]	1.4 ± 0.3[c]	F	47	4.5 x 3.3 x 1.6	*	124.5	0.96	19.5	15.3
	889741	1.9± 0.6[b]	5.6 ± 0.8[b]	9.5 ± 1.2[b]	5.2 ± 0.5[a]	1.8 ± 0.4[c]	M	41	3.4 x 1.3 x 1.6	1	1.9	1.89	2.39	10.5
	average	1.3 ± 0.6[b]	4.6 ± 1.0[b]	1.0 ± 0.2[c]	3.2 ± 1.9[a]	1.6 ± 0.1[c]								
highly	639205	2.6 ± 0.4[b]	5.5 ± 0.7[b]	2.3 ± 0.2[c]	8.9 ± 1.7[a]	3.2 ± 0.5[c]	F	82	7.6 x 7.3 x 6.3	8	3.77	14.7	17.9	34.6
	877082	3.3 ± 0.8[b]	6.9 ± 0.6[b]	3.1 ± 0.3[c]	1.0 ± 0.2[b]	4.2 ± 0.6[c]	F	91	5.5 x 3.3 x 2.9	10	2.98	2.5	14.7	25.5
	899833	3.9 ± 0.6[b]	8.9 ± 1.2[b]	1.9 ± 0.3[c]	6.5 ± 0.6[a]	3.3 ± 0.4[c]	F	48	7.5 x 2.5 x 2.1	15	12.5	13.9	15.2	13.2
	average	3.3 ± 0.6[b]	7.1 ± 1.7[b]	2.5 ± 0.6[c]	8.6 ± 1.9[a]	3.6 ± 0.5[c]								
moderately	639997	4.3 ± 0.5[b]	1.6 ± 0.3[c]	4.6 ± 0.5[c]	1.4 ± 1.5[b]	6.7 ± 0.6[c]	F	67	11.3 x 9.4 x 7.1	60	105.2	105.2	11.59	22.72
	877013	5.9 ± 0.9[b]	1.1± 0.2[c]	3.8 ± 0.4[c]	1.2 ± 0.2[b]	5.6 ± 0.7[c]	M	63	2.7 x 1.8 x 1.4	15	57.13	5.57	41.16	13
	893519	3.9 ± 0.7[b]	8.9± 1.6[b]	3.3 ± 0.4[c]	8.9± 1.7[a]	4.7 ± 0.5[c]	M	72	6.5 x 5.5 x 4.5	35	97.2	3.2	11.2	16.9
	average	4.7 ± 1.1[b]	1.2 ± 0.4[c]	3.9 ± 0.6[c]	1.2 ± 0.3[b]	5.7 ± 1.0[c]								
poorly	641332	5.6 ± 1.1[b]	2.8 ± 0.4[c]	6.7 ± 0.8[c]	1.9 ± 0.3[b]	1.0 ± 0.2[d]	M	54	9.5 x 9.4 x 6.3	60	150.1	2.4	247.4	112
	641361	8.1 ± 1.5[b]	3.2 ± 0.3[c]	8.9 ± 1.3[c]	2.1 ± 0.3[b]	1.3 ± 0.3[d]	M	59	18.7 x 14.1 x 8.8	60	1979	2.6	12.35	18.85
	892846	9.3 ± 1.9[b]	3.9 ± 0.3[c]	5.9 ± 0.9[c]	3.2 ± 0.3[b]	1.1 ± 0.2[d]	M	71	5.5 x 3.5 x 2.2	40	267	6.1	30.7	45.9
	average	7.7 ± 1.8[b]	3.3 ± 0.6[c]	7.2 ± 1.6[c]	2.4 ± 0.7[b]	1.1 ± 0.1[d]								

[a] × 10^{-19} mol;

[b] × 10^{-18} mol;

[c] × 10^{-17} mol;

[d] × 10^{-16} mol;

[e] The size of tumor, length × width × height with unit of cm;

[f] Ki67 staining, the proliferation index (%); higher Ki67 percentage indicates higher speed of tumor proliferation;

[g] AFP, ng/mL; 0.00~7.00 is clinically negative;

[h] CEA, ng/mL; 0.00~4.60 is clinically negative;

[i] CA125, U/mL; 0.00~35.00 is clinically negative;

[j] CA199, U/mL; 0.00~27.00 is clinically negative;

* The asterisk meant no data available for the clinical specimens.

TRANSPARENT METHODS

Materials

All the materials used in this study were at least of analytical grade except special notification. The ultrapure water was prepared with a Milli-Q system (18 MΩ, Millipore Filter Co., Bedford, MA, USA). Anhydrous copper sulfate $CuSO_4$ (purity > 99.9%), acetone, trifluoromethanesulfonic anhydride (Tf_2O, purity > 99%), pyridine (purity > 99.8%), acetic anhydride (purity > 99.9%) ammonium bicarbonate (NH_4HCO_3, purity > 99.9%), sodium bicarbonate ($NaHCO_3$, purity > 99.9%), sodium ascorbate (purity > 99%), 4-(2-hydroxyethyl)-1-piperazineethanesulfonic acid HEPES (purity > 99.5%), and ammonium acetate (CH_3COONH_4, purity > 99%) were purchased from *Aladdin* (Shanghai, China). Anhydrous L-galactose (1 gram) was purchased from Carbosynth. CO. Ltd. (Berkshire, UK). Dimethyl Formamide (DMF, purity > 99.9%) were purchased from *J&K Scientific* CO., Ltd. (Beijing, China). HPLC grade methyl alcohol (CH_3OH), acetonitrile (ACN), trifluoroacetic acid (TFA) and ammonium hydroxide solution (10% w/v), ethylene diamine tetraacetic acid (EDTA, purity > 99.9%), alkyne-Cy5 (*ALK*-Cy5, purity > 95%), 1-Phenyl-3-methyl-5-pyrazolone (PMP, purity > 99%), aminoguanidine (purity > 98%) and L-fucose (purity > 99%) were purchased from Sigma-Aldrich (Shanghai, China). 1,4,7,10-tetraazacyclododecane-1,4,7-tris(acetic acid)-10-(3-butynylacetamide) (*ALK*-DOTA) and 1,4,7,10-Tetraazacyclododecane-1,4,7-tris-acetic acid-10-maleimidoethylacetamide (*MAL*-DOTA) were purchased from Macrocyclics (Dallas, TX, USA). Concentrated HNO_3 (GR grade) was purchased from Merck KGaA (Darmstadt, Germany). High-purity europium oxides (purity > 99.999 %) were donated by Changchun Institute of Applied Chemistry of Chinese Academy of Sciences. Eu_2O_3 was dissolved in high purity HNO_3 to prepare $Eu(NO_3)_3$. ^{153}Eu-enriched Eu_2O_3 (99.8%) was purchased from Cambridge Isotope Laboratories, Inc. (Tewksbury, MA, USA). 2-Iminothiolane hydrochloride (Traut's Reagent, purity > 98%) was purchased from Sangon Biotech (Shanghai, China). Maleimide-polyethylene glycol-alkynyl (*MAL*-PEG-*ALK*, MW = 600, 1000, 2000, 3400, 5000 Da) were purchased from ZZBIO CO., Ltd. (Shanghai, China). Spin concentrator (Millipore Amicon Ultra-0.5, MWCO = 50 kDa) was purchased from Millipore (Bedford, MA, USA). The human hepatocellular carcinoma cell line (HepG2) and normal human hepatocellular cell line (HL7702) were obtained from the Institute of Cell Biology of Chinese Academy of Sciences (Shanghai, China). DMEM, RPMI 1640, fetal bovine serum (FBS), penicillin and streptomycin were purchased from ThermoFisher (Waltham, USA). The Cu(I) stabilized ligand, 2-(4-((bis((1-(tert-butyl)-1H-1,2,3-triazol-4-yl)methyl)amino)methyl)-1H-1,2,3-triazol-1-yl)acetic acid (BTTAA, purity > 95%) was purchased from Jena bioscience (Thuringia, Germany). The α1,2 fucosidase (20,000 mU/mL) and α1,3/4 fucosidase (4,000 mU/mL) were bought from New England Biolabs (USA) and the α1,6 fucosidase (1 U/mL) was purchased from Sigma-Aldrich (Shanghai, China).

Clinic samples. Totally 12 samples including 3 normal liver tissues and 3 highly, 3 moderately and 3 poorly differentiated HCC tissues were obtained from Xiamen University affiliated Zhang-Shan Hospital with consent of the ethics committee and the patients.

Instrumentation

A LC-10AD HPLC system (Shimadzu, Kyoto, Japan) equipped with an SPD-M10Avp UV detector, 200-μL sampling loop and a TechMate C18 column (10.0 I.D. × 200 mm in length, 5 μm particle size) was used for purifying the synthesized *ALK*-DOTA-Eu and *MAL*-DOTA-Eu using the mobile phases of A (H_2O containing 0.05 % V/V TFA) and B (ACN containing 0.05 % V/V TFA) with a gradient elution program starting from 95/5 to 10/90 A/B in 30 min at the flow rate of 4.0 mL/min. A Superdex 75 10/300 GL column (10 mm I.D. × 300 mm in length), 20-μL sampling loop and 50 mM ammonium acetate (pH 6.8) mobile phase was used for size-exclusion chromatography (SEC) to purify the synthesized *ALK*-PEG-MS2-DOTA-Eu at the flow rate of 0.8 mL/min. A SHIMADIU shim-pack column (10.0 I.D. × 200 mm in length, 5 μm particle size) was used to separate PMP-Fuc and PMP-Fuc*Az* with a gradient elution program starting from 80/20 to 70/30 CH_3COONH_4/ACN in 60 min at the flow rate of 0.25 mL/min. ESI-*q*TOF-MS Impact II (Bruker, Bremen, Germany) was used for identifying the compounds synthesized with the following instrumental parameters: nebulizer, 20 psi; dry gas, 0.4 L min^{-1}; dry temperature, 180 °C; capillary voltage, 4.0 kV; end plate offset, 0.4 kV. ELAN DRC-II ICP-MS (PerkinElmer, SCIEX, Canada) was

used for Eu-tagged Fuc*Az* quantification on the cell-surface under a bulk-cell sample introduction mode. The parameters were optimized for Eu determination as nebulizer gas, 0.88 L/min; auxiliary gas, 1.0 L/min; plasma gas, 15 L/min; RF power, 1200 W; dwell time, 100 ms; lens voltage, 7.2 V. A JEM-1400 field-emission electron microscope (TEM; JEOL, Japan) with 100 kV accelerating voltage was used for imaging the intact sphere of naked MS2-NH_2 and modified MS2-SH. ELAN DRC-II ICP-MS coupled with SEC (Superdex 75 10/300 GL column, 10 mm I.D. × 300 mm in length) was used for analyzing the amount of Eu tagged on MS2 with ^{153}Eu species-unspecific isotope dilution. Z36HK centrifuge (Hermle labortechnik, Wehingen, Germany) was used for purifying and concentrating bacteriophage MS2. Forma series II Water jacketed CO_2 incubator (Thermo scientific, USA) was used for cell cultivation. XB-K-25 chamber (Qiujing, Shanghai, China) was used for counting HL7702 and HepG2 cells. The CLSM imaging of HepG2 and HL7702 cells were performed on Zeiss LSM 780 confocal laser scanning microscope equipped with ZEN software (Carl Zeiss GmbH, Germany). After optimization of the *z*-axis scanning range with 0.1 μm resolution, -3.5 μm to + 3.5 μm at the z-axis was set for HepG2 and HL7702.

For single-cell analysis, a Harrick PDC-002 plasma cleaner (Harrick Plasm Inc., New York, U.S.A) and a spin coater were used in the preparation of microfluidic chips. A Phantom Micro C110 Camera (Vision Research Ltd., New Jersey, USA) on an Eclipse Ts2-FL inverted microscope (Nikon Corp., Tokyo, Japan) was employed for observing and recording the lined-up isolated cells. The single-cell ICP-MS platform was composed of (1) an oil-free passive microfluidic chip (OFPMC) with double alternating interconnected straight−curved−straight microchannels to manipulate single cells, together with (2) a direct infusion quartz capillary (365 μm O.D. × 75 μm I.D.) that was centrally inserted into a glass frame (7.0 mm O.D. × 4.0 mm I.D. × 208 mm in length) with a ventilation branch and a 400 μm I.D. end nozzle, serving as sample transport tube. At the end, the polyimide-layer of 2 mm protrusion was peeled off and retracted about 500 μm from the aperture of the nozzle to form an on-line micronebulizer. This direct infusion assembly served as (3) the central channel of the standard demountable ICP torch for making ion plume from the direct infused and lined-up single-cell for ICP-MS analysis. Before use, OFPMC was thoroughly flushed with 10 mmol/L NH_4HCO_3 Then the HL7702 and HepG2 cells suspension in 10 mmol/L NH_4HCO_3 solution were pumped into OFPMC through the cell sampling well and further sorted by a supplementary 10 mmol/L NH_4HCO_3 solution flow via a bifurcation joint in the second expended microfluidic channel. The lined-up cells with a certain internal time in-between were directly infused into ICP-MS via the direct infusion assembly. The optimum operating conditions of ICP-MS are: nebulizer Ar gas, 0.88L/min; auxiliary gas, 1.2 L/min; carrier gas, 0.4 L/min; plasma gas, 16 L/min; RF power, 1100 W; dwell time, 10 ms; lens voltage, 7.2 V. In this way, the transport efficiency of cells is 100% and detection efficiency in the single cell experiments is 86%.

Synthesis and characterization of Ac_4Fuc*Az*

The synthesis of per-acetylated azide-fucose (Ac_4Fuc*Az*) was carried out according to the previous reports with minor modifications (Scheme S1). (1) 2.22 mmol anhydrous L-galactose suspended in 10 mL dry acetone was treated with 5.63 mmol anhydrous $CuSO_4$ and 60 μL concentrated H_2SO_4 stirring overnight at room temperature. After removing the excess $CuSO_4$, neutralizing with $Ca(OH)_2$, filtering through Hirsch funnel and purifying through silica-gel (300~400 mesh) chromatographic column, we obtained 1,2,3,4-Di-*O*-isopropylidene-α-L-galactopyranose (Figure S1-3, yield 90%); (2) the obtained 1,2,3,4-Di-*O*-isopropylidene-α-L-galactopyranose (1.92 mmol) was added dropwise within 30 min into a mixed solution of 5:1 (V/V) dry dichloromethane/pyridine containing 4.23 mmol trifluoromethanesulfonic anhydride under stirring at 0 °C to activate the hydroxyl located at the C6 atom to get 1,2,3,4-Di-*O*-isopropylidene-6-trifluorome-α-L-galactopyranose (Figure S4) after dichloromethane dilution, twice ice-cold water washing and vacuum evaporation; (3) it reacted with 5-fold excess sodium azide in dry dimethylformamide under stirring for 15 h at room temperature. After dilution with dichloromethane, washing out unreacted sodium azide and other organic salts formed during the reaction with water twice, and evaporating out the solvent followed by purification on a silica-gel chromatographic column, 1,2,3,4-Di-*O*-isopropylidene-6-azido-α-L-galactopyranose (Figure S5-7) was obtained with a yield of 60%; (4) 6-azido-1,2,3,4-tetra-*O*-6-deoxy-α,β-L-galactopyranose (Figure S8) was obtained after deprotection in trifluoroacetic 9:1 acid/water (V/V) under stirring for 1 hour at room temperature, and neutralized with triethylamine

and evaporated together with toluene to get rid of water; (5) the obtained 6-azido-1,2,3,4-tetra-*O*-6-deoxy-α,β-L-galactopyranose was then acetylated with 1:1 pyridine/acetic anhydride (V/V) for 15 h at room temperature. Finally, we obtained 345 mg 6-azido-1,2,3,4-tetra-*O*-acetyl-6-deoxy-α,β-L-galactopyranose, Ac_4Fuc*Az* (Figure S9-10) with a yield of 47.5%, after went through the procedures of dilution with dichloromethane followed by washing with 1 M cold hydrochloric acid, saturated sodium bicarbonate and water in sequence, and vacuum evaporation then silica-gel chromatographic purification. All the intermediates and final product Ac_4Fuc*Az* were characterized with high resolution ESI-qTOF-MS and NMR to confirm success of the synthesis.

Synthesis and characterization of *ALK*-DOTA-Eu, *MAL*-DOTA-Eu and *ALK*-PEG-MS2-DOTA-Eu

Alkyne (*ALK*)-DOTA-Eu and maleimide (*MAL*)-DOTA-Eu were prepared according to the procedures reported by our group. Briefly, $Eu(NO_3)_3$ was added respectively into *ALK*-DOTA and *MAL*-DOTA at the mole ratio of 1.5:1 buffered by 200 mM HEPES (pH 6.8) at room temperature. *ALK*-DOTA-Eu and *MAL*-DOTA-Eu were purified on a semi-preparative HPLC with a TechMate C18-ST column (10.0 I.D. × 250 mm in length, 5 μm particle size) to get rid of excess Eu^{3+}. The purified *ALK*-DOTA-Eu (Figure S12) and *MAL*-DOTA-Eu (Figure S13) complexes were dissolved in HEPES (200 mM, pH 6.8) buffer solution to obtain their stock solutions of 5 mM each for later use. For *ALK*-PEG-MS2-DOTA-Eu, MS2 bacteriophage strain 15597-B1 purchased from the American Type Culture Collection (ATCC, Manassas, USA) was used to get empty MS2 capsid according to our previous work. Firstly, the amino group ($-NH_2$) on MS2 capsid (100 μM monomer) was first converted into sulfhydryl (-SH) using Traut's Reagent in $NaHCO_3$ buffer (pH 8.0) containing 5 mM EDTA with vortexing for 1 h at room temperature to obtain MS2-SH. It was characterized by ESI-qTOF-MS and transmission electron microscopy (TEM). Subsequently, MS2-SH was conjugated with *MAL*-DOTA-Eu and *MAL*-polyethylene glycol-alkyne (*MAL*-PEG-*ALK*) in the molar ratio of 1/2, 1/5, 1/10, 1/25, 1/50, 1/100, 0/1 (–SH/MAL) in 100 mM HEPES buffer (pH 6.8) containing 1 mM EDTA for 2 h vortexing at room temperature (Figure S14). The *ALK*-PEG-MS2-DOTA-Eu was purified by centrifugation (6000 × g) for 5 mins using spin concentrator (MWCO = 50 kDa) to remove unreacted *MAL*-PEG-ALK and/or *MAL*-DOTA-Eu, and characterized using ICP-MS. During which, different mole ratio between *MAL*-DOTA-Eu and the PEG of different length (PEG600, 1000, 2000, 3400 and 5000) was tested to get the most sensitive Eu signal (Figure S15-16).

Cell culture and cell viability assay

HepG2 and HL7702 were respectively cultivated in DMEM and RPMI 1640 supplemented with 10% FBS, 100 units/mL penicillin and 100 μg/mL streptomycin at 37 °C in a 5% CO2 humidified atmosphere. The synthesized Ac_4Fuc*Az* was added into the culture medium at a final concentration of 200 μM for 2 days cultivation to metabolically incorporate Fuc*Az* into the glycan-chain via cell's essential salvage pathway. The biocompatibility of Ac_4Fuc*Az* was then tested by a standard cell counting kit-8 (CCK-8). Seven cell samples (2.0×10^4 cell per well) were parallelly plated in a 96-well microliter plate and incubated with 0, 25, 50, 75, 100, 150, 200, 400, 800 μM Ac_4Fuc*Az*. After 48 h cultivation, the cells were washed with PBS five times and then analyzed by the CCK-8 cell-viability assay (Figure S11).

Metabolic incorporation of Fuc*Az* on the cell-surface

HepG2 and HL7702 cells of 2.5×10^6 were grown in the presence of 200 μM Ac_4Fuc*Az*. After 48 h cultivation in a 10 cm dish, the cells were washed with PBS and detached with trypsin and then counted by XB-K-25 chamber. 1.0×10^6 cells of HepG2 and/or HL7702 were collected, and the Fuc*Az* incorporated on the cell was bioorthogonally tagged with 10 μM *ALK* -DOTA-Eu via click reaction under the conditions of 0.5 mM Cu(I) stabilizer BTTAA, 0.1 mM $CuSO_4$, 1 mM aminoguanidine and 2.5 mM sodium ascorbate at pH 7.4 buffered by 100 mM HEPES at room temperature for 30 min. Besides, the control experiments of without Ac_4Fuc*Az* metabolic incorporation and/or without *ALK*-DOTA-Eu tagging, with Ac_4Fuc*Az* incorporation but without *ALK*-DOTA-Eu tagging, and with *ALK*-DOTA-Eu tagging but without Ac_4Fuc*Az* incorporation were also

performed to investigate the metabolic FucAz incorporation and the specificity of element-tagging. It should be noted that the unreacted free *ALK*-DOTA-Eu must be removed. For this, 100 mM HEPES buffer (pH 6.8) containing 1 mM EDTA was used to wash out the possible free *ALK*-DOTA-Eu seven times and each washing run lasted for 30 seconds with gently shaking (Figure S18). In parallel, *ALK*-Cy5 (10 μM) (λ_{Ex} = 633 nm and λ_{Em} = 647) was used for labeling the cell-surface FucAz and hoechst 33342 (2'-(4-ethoxyphenyl)-5-(4-methyl-1-piperazinyl)-2,5'-bi-1H-benzimidazole trihydrochloride, 5 μg/mL) (λ_{Ex} = 405 nm and λ_{Em} = 433 nm) for nuclei staining to image the cells under a Zeiss LSM 780 laser scanning confocal microscope equipped with a 40 x oil-immersion objective lens (Figure S19).

Quantification of the Fuc*Az* on cell surface of HepG2 and HL7702 cell lines

After the cultivation with Ac_4Fuc*Az* for 48 h in 6-well plates and necessary washing, HepG2 and HL7702 cells tagged with 10 μM *ALK*-DOTA-Eu in pH 7.4 buffered 100 mM HEPES for 30 min at the room temperature via the click reaction as mentioned above. Subsequently, the cells (1.0×10^6 counted by XB-K-25 chamber) were further washed five times and centrifuged at 500 x g for 3 mins. They were determined using ^{153}Eu-SUID-ICP-MS under the conventional bulk-cell sample introduction mode, after the cells were dissolved in 2% HNO_3 and $^{153}Eu(NO_3)_3$ spike (6.53×10^{-12} mol) was added. Due to 1:1 stoichiometrically clickable tagging of *ALK*-DOTA-Eu to Fuc*Az* (Figure S17), the determined amount of Eu was that of Fuc*Az* on the cell-surface. Amount of Fuc*Az* was calculated via the following isotope dilution equation:

$$N_S^{FucAz} = N_S^{Eu} = N_{Sp}^{Eu} \cdot \frac{R_m A_{Sp}^{153} - A_{Sp}^{151}}{A_S^{151} - R_m A_S^{153}} \rightarrow 6.53 \times 10^{-12} \cdot \frac{0.002R_m - 0.998}{0.4781 - 0.5219R_m} ,$$

where N_S^{FucAz}, N_S^{Eu} and N_{Sp}^{Eu}denote the number of Fuc*Az* (mol) and the Eu-tagged on the cell-surface, and Eu in the spike solution; A_S^{151} and A_S^{153} are the isotopic abundance of ^{151}Eu (47.81%) and ^{153}Eu (52.19%) tagged on the cell-surface; and A_{Sp}^{151} and A_{Sp}^{153} are those in the spike solution (0.2% and 99.8%). R_m is the isotope ratio of ^{151}Eu/^{153}Eu which can be precisely measured using ICP-MS at the dwell time of 100 ms. The determined Fuc*Az* on the cell surface divided by the number of cells to obtain the average Fuc*Az* on per cell.

In order to quantify the total Fuc*Az* and its specific glycosidic linkages on a single cell, the cells were tagged with 10 μM *ALK*$_{101}$-PEG2000-MS2-DOTA-Eu$_{979}$ nanoparticles. For total single cell surface Fuc*Az* analysis, after washing out the unreacted *ALK*$_{101}$-PEG2000-MS2-DOTA-Eu$_{979}$ and setting a shorter dwell time of 10 ms, they were analyzed on the direct-infusion of lined-up single-cell ICP-MS platform previously established in our laboratory. The cell density was 2.0×10^5 cells/mL and keeping the cell sampling flow rate at 6 μL/min, while the supplementary flow at the flow rate of 7 μL /min for stabilizing the inertial flow velocity that further pushing forward the lined-up cells with the interval time was over than 13 ms. Data collection and processing were using an iterative algorithm based on the three times standard deviation (3σ) to distinguish single cell events regarding ^{153}Eu from background signals. The average signal value and standard deviation of the entire data set were calculated, and the data higher than the sum of 3σ and the average values were collected as an independent cell event. The Fuc*Az* on single HL7702 and HepG2 were obtained via the determination of ^{153}Eu from 3000 valid cell events (Figure S21). As for the different linkage Fuc*Az*, the cells were respectively treated with linkage-specific fucosidases to release their corresponding linkage-specific fucose, the remained linkage-specific Fuc*Az* on the cell-surface was determined on the direct-infusion of lined-up single-cell ICP-MS platform. For example, the other types of fucosylation was firstly quantified by employing the α1,2, α1,3/4 and α1,6 fucosidases (5 μL each) at 37°C for 2 hours to release α1,2, α1,3/4 and α1,6 fucose linkages on the oligosaccharide chains according to the manufacturer's instructions. After centrifugation to discard the supernatant (500 × g, 3 min), the other types of Fuc*Az* remained on the cell-surface were determined through the quantification of the tagged Eu on the direct-infusion of lined-up single-cell ICP-MS platform. The same procedures were applied to the determination of α1,2, α1,3/4 and α1,6 FucAz on a single cell (Figure S22).

Quantification of the Fuc*Az* on the cell surface of the clinical normal and hepatocellular carcinoma (HCC) cells

The normal (paracancerous) and HCC tissues obtained from Xiamen University affiliated Zhong-Shan Hospital that were resected during surgical operations. These specimens were immediately cut up into pieces and cleaned with D-Hanks buffer (100 mM, pH 7.4) and Red Blood Cell Lysis Buffer (volume 3:1) to wash up the residual red blood cells and other appendant tissue sundries. The treated specimens were digested with 1.5 mL collagenase buffer (0.25 mg/mL in 100 mM PBS, pH 7.4) at 37 ºC for 2 hours, and then filtered to receive the single HCC cells for further cell cultivation experiments. The obtained single cells were cultivated in the presence of 200 μM Ac_4Fuc*Az*. After 48 h cultivation in a 10 cm dish, the cells were washed with PBS and detached with trypsin, and then counted by XB-K-25 chamber. 1.0×10^6 cells of HepG2 and/or HL7702 were collected for the Fuc*Az* incorporation. Afterwards, they were bioorthogonally tagged with 10 μM *ALK*$_{101}$-PEG200-MS2-DOTA-Eu_{979} via the click reaction under the same conditions as those performed for HepG2 and/or HL7702. The Eu-tagged Fuc*Az* and its fucosidic linkage-specific motifs were quantified on the direct-infusion of lined-up single-cell ICP-MS platform.

Evaluation of the metabolic Fuc*Az* incorporation efficiency

Metabolic incorporation efficiency of Fuc*Az* on the surface of HepG2 and HL7702 cells was determined using the standard monosaccharide 1-Phenyl-3-methyl-5-pyrazolone (PMP) derivatization HPLC method with some modifications (Suzuki et al., 2003). The Ac_4Fuc*Az* cultivated HepG2 and HL7702 cells (1.0×10^7 cells) were treated with 50 mM HCl at 100 °C for 4 h and the cell surface glycan were hydrolyzed to monosaccharides. By discarding the cell pellets, the supernatant containing monosaccharides were neutralized with 0.1 M NaOH and desalted with a Sep-Pak C18 cartridge to obtain the pure monosaccharides. Before HPLC analysis, PMP derivatization was performed in 400 μL of CH_3OH/H_2O (1:1) containing 0.3 M NaOH and 0.5 M PMP under gentle vortexing for 30 mins at 70°C in darkness. Afterwards, the solution was neutralized with 0.3 M hydrochloric acid, and then evaporated under reduced pressure. Water and chloroform (1:1) were added to the residue, and the mixture vortexed vigorously to transfer the excess PMP reagent to the chloroform layer, then the aqueous layer evaporated to dryness and redissolved in methanol-water (1:1 v/v). Subsequently, the PMP-derivatized monosaccharide samples (20 μL each) were injected into an HPLC system with CH_3COONH_4 and ACN as the mobile phase with a gradient elution program starting from 80/20 CH_3COONH_4/ACN to 70/30 CH_3COONH_4/ACN in 60 min at the flow rate of 0.25 mL/min and detected at the maximum absorption wavelength λ_{max} = 245 nm. The Fuc*Az* metabolic incorporation efficiency (%) was measured by the peak area of Fuc*Az* divided by the sum of the peak areas of Fuc*Az* and Fuc (Figure S23).

Supplemental References

Suzuki, S., Ishida, Y., Arai, A., Nakanishi, H., and Honda, S. (2003). High-speed electrophoretic analysis of 1-phenyl-3-methyl-5-pyrazolone derivatives of monosaccharides on a quartz microchip with whole-channel UV detection. Electrophoresis *24*, 3828-3833.